Validation of the Space-Time Variability of African Easterly Waves Simulated by the CNRM GCM.

Céron J.-P., Guérémy J.-F.

Validation of the Space–Time Variability of African Easterly Waves Simulated by the CNRM GCM

J. P. CÉRON AND J. F. GUÉRÉMY

Ecole Nationale de la Météorologie–Unité de Météorologie Tropicale, Météo-France, Toulouse, France

(Manuscript received 14 April 1995, in final form 29 September 1998)

ABSTRACT

The ability of the Centre National de Recherches Météorologiques (CNRM) general circulation model (GCM) to properly simulate the space–time variability of the African easterly waves (AEWs) has been examined over the period 1982–88. The relative vorticity at 850 hPa in the analyses of the European Centre for Medium-Range Weather Forecasts analyses has been compared with the CNRM GCM simulations carried out in the framework of the Atmospheric Model Intercomparison Project. Detailed results of two statistical diagnoses used in this study have been presented for the selected year of 1985 in order to evaluate against the results of extensive studies available for this year.

First, with the help of a space–time spectral analysis, it has been shown that the GCM produces only one main variance maximum for the waves located between the two analyzed variance maxima (consistent with the northern and southern components associated with AEWs). The waves in the GCM propagate more slowly than those from the analyses, mainly because of greater periods in the GCM. There is a qualitative agreement between the simulation and the analysis in terms of the seasonal evolution of the location and intensity of the variance maximum. Barotropic and baroclinic energy transfers seem to be quite correctly represented.

Second, using a complex empirical orthogonal functions analysis, the existence of two main modes of variability of AEWs has been illustrated. A first hypothesis is proposed for the two modes' interpretation. The second mode seems to be well linked to the interannual rainfall variability over West Africa. A low-frequency modulation of the wave activity exists in the analyses. This modulation is only qualitatively duplicated in the GCM. Interannual variability of the variance shown by the analyses is quite well reproduced by the GCM, particularly the variance seesaw of the two main modes between dry and wet years. Nevertheless, the GCM does not seem able to correctly simulate the pattern of atypical years, such as 1987. Finally, by projecting the GCM dataset on the eigenvectors of the analyses, it has been shown that GCM time discrepancies could influence the quality of the space representation of the AEWs.

1. Introduction

The existence of synoptic-scale disturbances that propagate toward the west from western Africa to the Caribbean during the period from late May until October has been noted for many years. One of the first studies on these waves over Africa was done by Shove (1946) using Nigerian conventional upper-air observations. Carlson (1969a) was the first author to use analyses of surface and upper-air data, from the summer of 1967, in order to track the waves. Burpee (1972) made spectral analyses of the meridional wind at several stations to specify the source regions. The Global Atmospheric Research Program (GARP) Atlantic Tropical Experiment (GATE) was undoubtedly the major event that vastly improved our knowledge and understanding of African easterly waves (Burpee and Reed 1982). Wave composite analyses (e.g., Reed et al. 1977) have provided a clear picture of the wave structure and wave energetics that have been used to understand the relationship between the wave and the African easterly jet (Norquist et al. 1977). In the 1980s, Reed et al. (1988a) demonstrated that objective analyses were able to reproduce reasonably well the African easterly waves (hereafter called AEWs), and the use of satellite data together with these analyses has improved our knowledge of the relationship between the waves and the cloudiness (e.g., Duvel 1990).

AEWs over the African continent are characterized most of the time by two vorticity maxima located on each side of the African easterly jet (AEJ) core, at slightly lower levels (i.e., around and under 700 hPa; Carlson 1969b; Burpee 1974). These two components of the AEWs may or may not be present (in terms of the intensity of their low-level vorticity maxima) at the same time, depending upon their respective life cycles (Reed et al. 1988a). The northerly component of the AEWs is

Corresponding author address: Dr. Jean-Pierre Céron, Ecole Nationale de la Météorologie–Unité de Météorologie Tropicale, 42 avenue G. Coriolis, F31057-Toulouse Cedex 1, France.
E-mail: Jean-Pierre.Ceron@meteo.fr

usually associated with larger vorticity anomalies at low levels but is limited in height at around 600 hPa, notably in terms of the vertical velocity field; the wave axis tilts eastward (westward) with height below (above) the AEJ (Reed et al. 1977). The southerly component of the AEWs has a deeper structure with a mid- to upper-tropospheric level maximum in the vertical velocity field; the wave axis tilts in the same direction as for the northerly component, the tilt being less (more) pronounced below (above) the AEJ (Reed et al. 1977). Due to these two components, two preferred tracks of vorticity maximum (used as a marker of the AEWs) do exist over the African continent at low levels, one located between 8° and 15°N and a second one located between 17° and 25°N. The southerly component has been the most extensively studied (due to the availability of observations and an apparent relationship between precipitation and possible generation of tropical cyclones). The observational studies referred to above have shown that the southerly component of the waves forms somewhere between 20°E and 0° and reaches its largest amplitude around the west coast of Africa with the maximum development occurring between 10°E and the west coast (Albignat and Reed 1980). This southerly component generally decays over the ocean, but it can also regenerate into tropical cyclones. The northerly component forms between 10°E and 10°W and reaches its largest amplitude near the west coast; most of the time it turns southward and generally decays over the ocean, tending to merge with the southerly component (Nitta and Takayabu 1985; Reed et al. 1988b). From GATE studies, it appeared that the waves have a wavelength of between 2000 and 3000 km, a period of 3 to 5 days, and therefore a westward phase speed of about 7 m s^{-1}.

The association of convective activity and precipitation with the waves has been studied for many years; but with the availability of satellite observations, it became possible to merge the satellite pictures with meteorological analyses to visualize a continuous space–time evolution of the interaction between the waves and the clouds. There is a maximum of rainfall and cloud cover ahead (behind) of the trough axis for the southerly (northerly when clouds do occur) component of AEWs (Carlson 1969a; Reed et al. 1977). Payne and McGarry (1977) presented similar results (using the GATE dataset for the southerly waves) for large cloud clusters but showed that smaller clusters occured most frequently near the ridge axis; in particular, squall lines seemed to appear preferably ahead of the wave trough. Duvel (1990) has shown that the largest deep convective activity is located at and ahead of the trough around 8°N during the years 1983–85. But around 18°N the deep convection has a primary maximum east of the trough. Finally, Toledo Machado et al. (1993) have shown that the largest size clusters appear at and ahead of the wave trough when the wave amplitude is the largest.

Concerning our understanding of the physical mechanisms involved in the life cycle of the waves, several papers have been published so far. The main results on this topic were presented after GATE. A comprehensive study of the energetics of the waves was carried out by Norquist et al. (1977), in which they showed that both barotropic and baroclinic conversions between the wave and the AEJ could explain a large part of the life cycle of the waves, the baroclinic conversion being the largest over land. The role of these dynamical instabilities of the AEJ in the life cycle of the AEWs explains the possible existence at the same time of two low-level vorticity maxima, on each side of the jet. The southerly component of the AEWs interacts very often with deep convection, which results in a deeper and quite different vertical structure than that of the northerly component (Reed et al. 1977). Several authors have conducted linear instability studies, using mainly observed data on the AEJ at 5°E (which is a location of mature waves), which have given unstable modes dominated by barotropic energy conversions (Rennick 1976; Mass 1979). More recently, Thorncroft and Hoskins (1994a) and Paradis et al. (1995) have published similar studies, but the inclusion of a simple cumulus parameterization seemed to increase the growth rate and favor the baroclinic conversion. Thorncroft and Hoskins (1994b) have shown that the nonlinear behavior of an easterly wave normal mode is dominated by a baroclinic conversion (except for the generation still dominated by a barotropic conversion), when both conditional instability of the second kind and boundary layer parameterizations were included.

A significant interannual variability in the amplitude and location of the waves does exist (Reed et al. 1988b). However, this topic has not been much addressed because of the lack of a long and continuous (in space and time) dataset.

There are only a few studies on simulated AEWs produced by primitive equation models including a comprehensive physics package. Walker and Rowntree (1977) have integrated a limited area model over 10 days, and they have shown that the maintenance of the wave eddy kinetic energy was mainly due to baroclinic conversion, once the wave formed. Estoque et al. (1983) have simulated the summer of 1974 using the Goddard Laboratory for Atmospheric Sciences general circulation model (GCM); a synoptic analysis for the month of July has shown that the behavior and structure of the simulated disturbances were similar to those observed with, in particular, the intensification of the waves just south of Lake Chad (for waves already formed somewhere in the east). Reed et al. (1988a,b) have evaluated the performance of the European Centre for Medium-Range Weather Forecasts (ECMWF) system in analyzing and forecasting (up to 48 h) the easterly waves; the simulated waves appeared to be slower than those analyzed. Druyan and Hall (1994) have determined the model representation of the waves in summer simulations of the Goddard Institute for Space Studies GCM.

The wave characteristics were realistic except for the phase speed, which was too slow as in the previous study. However, the simulated wave amplitude decreases too much in September compared to observations, and the precipitation was enhanced east of the wave trough contrary to observational evidence.

The aim of this study is to determine the ability of the Centre National de Recherches Météorologiques (CNRM) GCM to reproduce the space–time variability of the AEWs, with the help of two complementary objective methods [a space–time spectral analysis, hereafter called STSA, and a complex empirical orthogonal functions (CEOF) analysis, hereafter called CEOFA]. This validation study has been carried out using the ECMWF analyses as the reference (for the years 1982–88). Thus, the space–time variability of the AEWs as seen in the analyses will be discussed first, before the validation process itself (i.e., GCM simulation against ECMWF analysis).

This work is a preliminary study to precipitation monthly forecasts insofar as easterly waves are the smallest dynamical phenomena (which modulate rain-bringing systems and might be modulated by lower-frequency oscillations) that might be simulated by the model. Indeed, it is necessary to determine if the GCM is able to reproduce statistically the easterly wave space–time variance (with its interannual and intraseasonal variability) before testing the prediction ability (i.e., the capacity to reproduce the phase and amplitude evolution). The prediction hope is related to the low-frequency modulation of the easterly wave amplitude, exhibited in this paper.

After a discussion of the data and methods used in this study in section 2, the results obtained with the help of STSA (CEOFA) will be presented in section 3 (section 4), followed by the conclusions in section 5.

2. Data and methods

a. Data

The data used in this study are, on the one hand, the ECMWF analyses, widely described and used in many reports or papers [see ECMWF (1988) for a complete review], and, on the other hand, simulated data provided by the CNRM GCM integrated over the Atmospheric Model Intercomparison Project (AMIP) period, namely, 1979–88. The simulation was performed using observed sea surface temperature and observed ice pack extension on a monthly basis in the AMIP context (Gates 1992).

The version of the GCM (so-called Emeraude) used for the AMIP experiment is a spectral model with a T42 triangular truncation in the horizontal and an L30 discretization for the vertical, including 21 levels in the troposphere. This model includes a classic set of physical parameterizations such as radiative processes, convection using a mass flux scheme, and surface processes (Mahfouf 1993).

Looking at the climatology of the model, one may assume a rather good simulation of the summer monsoon flows in the Northern Hemisphere. However, focusing over West Africa, a northward shift of rainfall has been noticed (not shown). This discrepancy is linked to problems of surface processes representation (more precisely, albedo values that are too low over Sahara and sub-Sahara regions) and feedback effects between physical and dynamical processes. The albedo field has been improved since then.

Concerning ECMWF analyses, as mentioned by Duvel (1990), they are probably a better basis for GCM validation than local measurements as well as the best available information over regions with a poor observational network. The major problems in the use of such a dataset over a long period like that of AMIP are revisions of the analysis scheme, resolution changes, or parameterization improvements. A major change in the analysis scheme occurred in May 1984 (Shaw et al. 1987). A complete review of ECMWF parameterization changes has been done by Tiedke et al. (1988), including one of the most important changes introduced in May 1985. This change introduced the shallow convection, a revision of deep convection, a new cloud cover scheme, and an increase of the horizontal resolution (from T63 to T106). Finally, the use of divergent constraint in the analysis increments has been implemented in the wind analyses in January 1988.

The effects of the change implemented in May 1984 are not clearly documented for tropical regions. Nevertheless, one can expect, on one hand, a better accuracy of the analyzed winds since 1984 and, on the other hand, as highlighted by Shaw et al. (1987), less impact in the lower than in the upper troposphere.

Before the major change of May 1985, the main forecast errors (Tiedke et al. 1988) were a drying of the tropical troposphere, a cooling of the tropical troposphere, a weakening of the Hadley circulation, a weakening of subtropical highs, and a poleward and upward displacement of subtropical jets. Forecasts benefitted much from these parameterization and resolution changes. However, the differences in the wind analyses were quite modest (Tiedke et al. 1988), particularly looking at the low levels. The main modifications were a slight strengthening of the trade winds and an increase of convergence near the ITCZ.

Finally, the change of January 1988 (Unden 1989) seemed to have a low impact on vorticity, which will be the main parameter for our study.

Thus, we consider that the wind analyses are quite homogeneous and have a rather good quality over the period 1982–88, which enables us to use them as ''references'' in order to validate the results from the GCM. One can notice (Lare and Nicholson 1994) that these seven years are very different regarding rainfall over West Africa and the global interannual variability (El Niño/La Niña years).

The data were extracted every 6 h, using the ECMWF

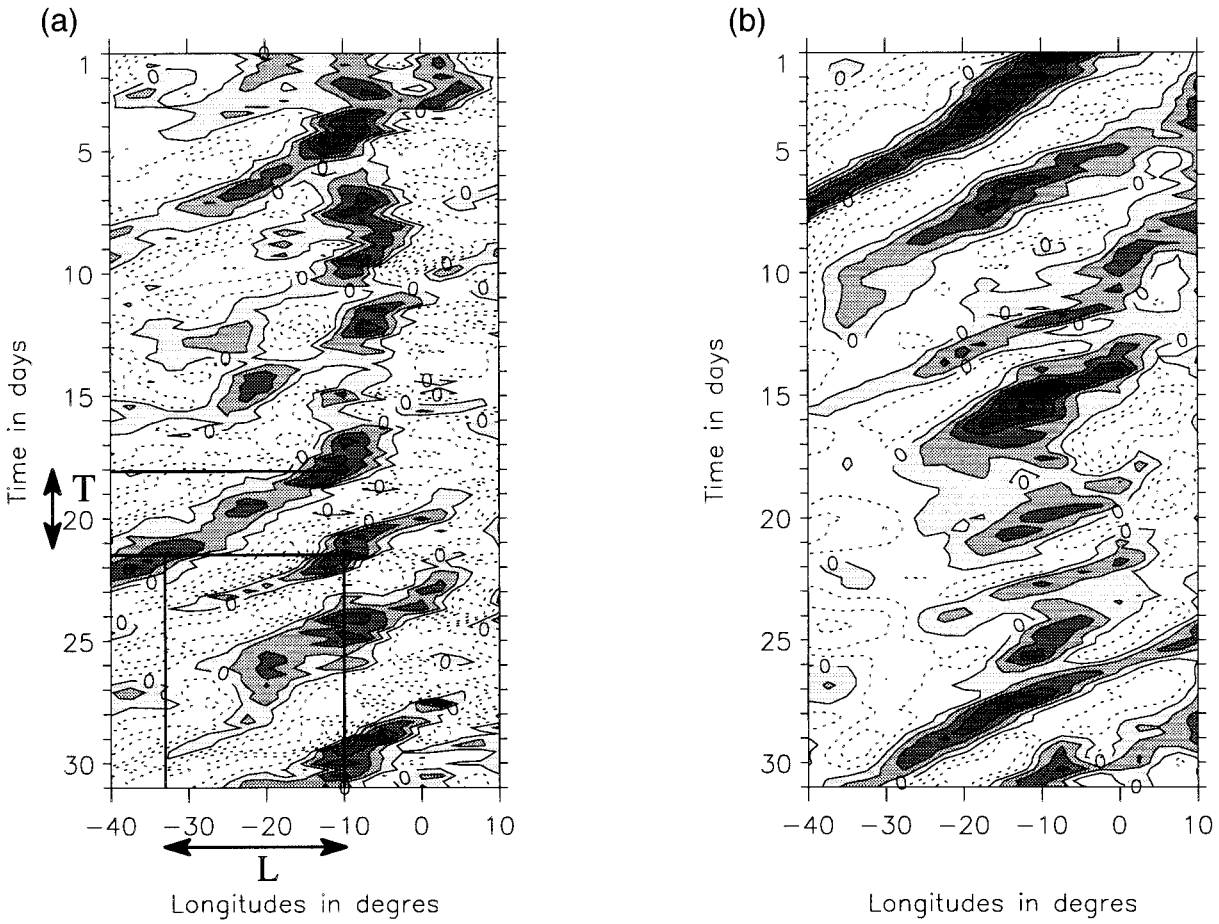

FIG. 1. Hovmöller diagram of relative vorticity (in s^{-1}) at 850 hPa averaged between 0° and 20°N for Aug 1985; (a) ECMWF, (b) CNRM GCM. Gray areas indicate cyclonic vorticity. Contour interval is 4×10^{-6} s^{-1}. T represents the period of the wave and L its wavelength.

archive system, over the May–October period, on a regular grid with a 2.5° × 2.5° mesh consistent with the horizontal resolution of the GCM. The May–October period has been chosen to focus on the major period of AEW activity over West Africa (Hastenrath 1991). Consequently, for each year, we have 736 observations representing 184 days from 1 May to 31 October.

As suggested by Reed et al. (1977, 1988a), we used the relative vorticity at 850 hPa in order to identify the activity of AEWs. Figure 1 shows time–longitude diagrams of the raw vorticity (averaged from 0° to 20°N), for the month of August 1985. The westward propagation of waves is clearly pointed out both in the analyses and in the GCM. Looking at the analyses, a positive/negative dipole of vorticity appears, near 5°E, on 20 August and propagates to the western part of the domain. The wavelength of the wave can be estimated at around 2500 km and its period at around 3.5 days, which is consistent with AEW characteristics (Reed et al. 1977). Roughly speaking, the GCM seems to simulate waves in the same range of period and wavelength, even if the period tends to be larger and the origin of the waves tends to be farther to the east. Those discrepancies will be discussed hereafter. Additionally, GCM results indicate a link between the 0°–20°N averaged vorticity and the 0°–20°N averaged rainfall (Céron and Guérémy 1994). Rainfall tends to propagate westward just before the cyclonic cells of vorticity, according to the AEW composite analysis done by Reed et al. (1977).

The vorticity parameter has been used in both raw and filtered forms. The chosen filter was a fourth-order Butterworth's bandpass filter (Murakami 1979) associated with a 2.5–6-day bandwidth. This filter was used twice, with one step ascending the time series and the other descending, in order to prevent phase shifts between raw and filtered data. The response of the filter (Fig. 2) is very sharp and gives a very good response in the 3–5-day bandwidth, which is the range of periods of AEWs. In fact, the characteristics of the bandwidth have been chosen by looking first at results from STSA (see section 3).

The space domain used depends on the method. For STSA we chose a domain as large as possible because of wavenumber representation (Fig. 3). For CEOFA we used a domain more focused on the AEW location (Fig.

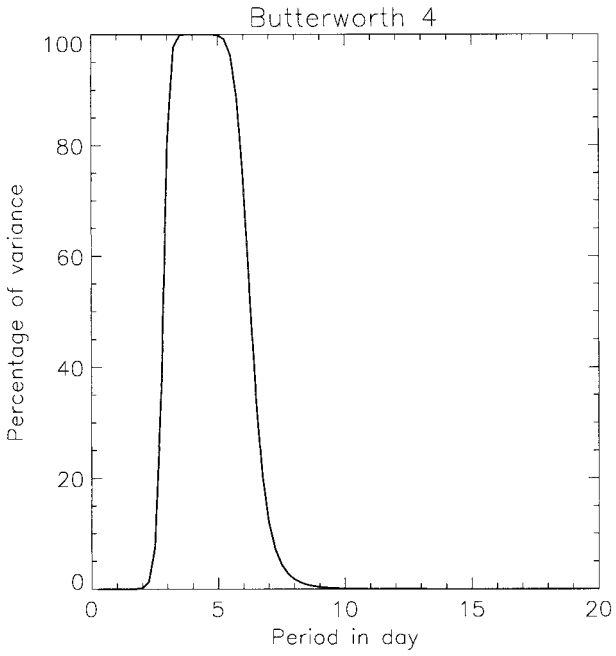

FIG. 2. Filter response, in percent of variance, of the fourth-order Butterworth filter for the chosen bandwidth vs period.

3); consequences of this choice will be discussed in the next section.

b. Methods

Two methods have been applied in order to quantify and compare space–time variability both from the analyses and from the GCM. Each method has been applied year by year because first, there is no evidence a priori that there are stable patterns in AEWs, particularly with regard to the interannual variability of rainfall over West Africa. Second, we are interested in quantifying the seasonal variability. Last, a year-by-year study will be a good test of robustness for our expected results. We have carefully evaluated the methods using data from the year 1985 because very extensive and useful studies have been published for this year by Reed et al. (1988a,b). Then, we have verified the relevance of the methods and the stability of the conclusions for the other years.

First we applied STSA on the raw dataset. We extended a method proposed by Hayashi (1977, 1979, 1982) by including a two-dimensional space representation. An advantage of Hayashi's scheme is that it allows a partition between standing and traveling wave variance and that it is suitable to make quantitative variance comparisons. This method is based on space–time Fourier decomposition, and we can summarize the different steps as follows (Hayashi 1977). First, one applies a space Fourier transform both in zonal and meridional directions. Second, one computes the time cross-spectrum between the real and imaginary parts of the previous space spectral coefficients (i.e., the cosine and sine space coefficients), which gives the time cross-spectrum between waves moving in opposite direction. Summing the spectral power densities over all meridional wavenumbers, these calculations give a space–time spectrum where one can separate westward and eastward moving waves. Third, according to Hayashi's method, one can obtain a partition between traveling and standing waves.

The first application of Hayashi's method (Hayashi 1977) was performed on a zonally periodic domain. Due to the Fourier function's decomposition, application of the method on a limited area requires some precaution in order to assume quasiperiodic data both in space and time. Therefore, we removed the linear trend both in space and in time domain before computing STSA. Additionally, we computed a space representation of the time variance as proposed by Hayashi (1979), this calculation being done over the space–time spectral window of the AEWs.

Then we used a CEOFA, which is based on empirical mode decomposition and is particularly useful for studying traveling phenomena. Introduced by Wallace and Dickinson (1972) in meteorological applications, CEO-

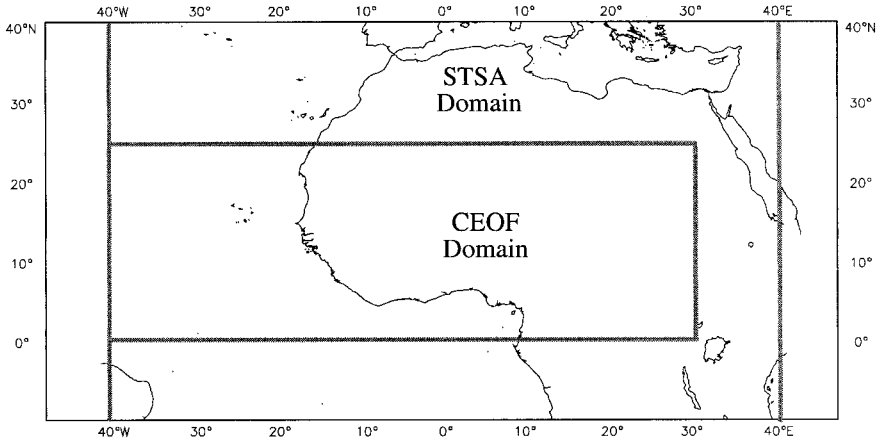

FIG. 3. Space areas used for the STSA method and the CEOFA method.

FA leads to a decomposition of a space–time signal in the following form:

$$X(M, t) = \sum_{j=1}^{p} A_j(M)B_j(t) \cos(\omega_j t + k_{j,X}X + k_{j,Y}Y),$$

where

$X(M, t)$ is the space–time signal,
M is the space variable corresponding to the zonal (X) and meridional (Y) directions,
t is the time variable,
$A_j(M)$ is the module of the CEOF j (CEOF n° j),
$B_j(t)$ is the module of the complex principal component j (CPC n° j),
$\omega_j = 2\Pi/T_j$ is the pulsation of the CPC n° j (corresponding to the period T_j),
$\omega_j t = \varphi_j(t)$ represents the time phase of the CPC n° j,
$k_{j,X} = 2\Pi/\lambda_{j,X}$ corresponds to the zonal wavenumber of the CEOF n° j,
$k_{j,Y} = 2\Pi/\lambda_{j,Y}$ corresponds to the meridional wavenumber of the CEOF n° j, and
$k_{j,X}X + k_{j,Y}Y = \Phi_j(M)$ represents the space phase of the CEOF n° j.

Looking at a traveling wave $X(M, t) = A(M)B(t) \cos[\varphi(t) + \Phi(M)]$ as a matter of evidence, the previous decomposition is particularly relevant for this kind of phenomenon.

To compute CEOFs, one can use two different methods. The first one uses the Hilbert's transform (Barnett 1983). This leads one to use a complex form of the real signal and consequently to compute the complex covariance matrix of the complex signal. CEOFs are given by eigenvectors (and associated eigenvalues) of the complex covariance matrix.

The second way, corresponding to the method proposed by Wallace and Dickinson (1972), uses time cross-spectrum computations. Then, integrating the cross-spectrum matrix over frequencies, we can obtain the complex covariance matrix. The different methods have been compared in Déqué (1986), and we chose to compute CEOFs using the cross-spectrum matrix. More precisely, we calculated the cross-spectrum using a sample method taking into account some advantages highlighted by Déqué (1986). So, we have split the six months of observations per year in eight samples corresponding to 92 observations each, that is to say, 23 days by sample (four observations per day). The length of each sample has been chosen considering the characteristic periods of AEWs (around 4 days) and the problems linked to the Fourier decomposition (namely, we must have enough periods in each sample in order to have a rather good estimation of the waves).

As recommended by Déqué (1986), we weighted data at each grid point taking into account the spherical surface of the domain. This led us to introduce a weight that is proportional to the root of the cosine of the latitude.

Just before applying the CEOFA method, we used a classic empirical orthogonal function analysis (EOFA), in order to provide an easier calculation of CEOFs and to look at the ability of this factorial method to identify AEWs. Additionally, we made some sampling sensitivity tests both in space and time domains. Looking at the sensitivity of the methods to the space domain, we tested four different domains. One can see in Figs. 4a and 4b that the patterns of EOFs are quite stable from the larger domain (used for STSA) to the smaller one (finally retained for EOFA and CEOFA). In fact, the main differences between different analyses done are in the rank and percentage of variance corresponding to associated eigenvalues.

In the same way, results from raw and filtered data are also quite comparable both in space (for EOFs and CEOFs, not shown here) and time domains [for principal components (PCs) and CPCs]. As shown in Figs. 5a and 5b, the main difference came from the smoothing effect of the filter in the time domain. It has been noticed that the space phases (not shown here) are less noisy for filtered data.

3. Results from the space–time spectral analysis

a. Wave spectra

Figure 6 shows the space–time spectra (the all-space domain and May–October 1985) of the traveling waves for ECMWF (top panel) and the GCM (bottom panel). These diagrams give the power density versus the frequency (negative for eastward propagating phenomena) in the abscissa and the zonal wavenumber in the ordinate. On both spectra, there are several maxima of power density between 36 and 60 in time (3–5 days) for westward propagating phenomena and 2 and 4 in space (2200–4400 km). This spectral window is consistent with what has been found by other authors (e.g., Reed et al. 1988b) for the AEWs. However, the model variance maxima tend to be located toward lower frequency compared to the analysis variance maxima. Indeed, the secondary maximum of power density around 37 (5 days) is larger in the spectrum of the simulated data (Fig. 6). The order of magnitude of the model variance cumulated in the AEW spectral window is the same as that of the analysis variance (this topic will be discussed in more detail in section 4). Interestingly, there are also local maxima on both spectra for much lower frequencies of around ± 5 in time (37 days, for eastward and westward propagating oscillations) and for the first wavenumber. The same spectra computed for standing plus traveling waves (not shown) allow us to say that traveling wave variance represents 23% of the variance of all the waves, but more than 70% of the AEW variance. We have noticed the same kind of pattern for the other years, indicating a good similarity between anal-

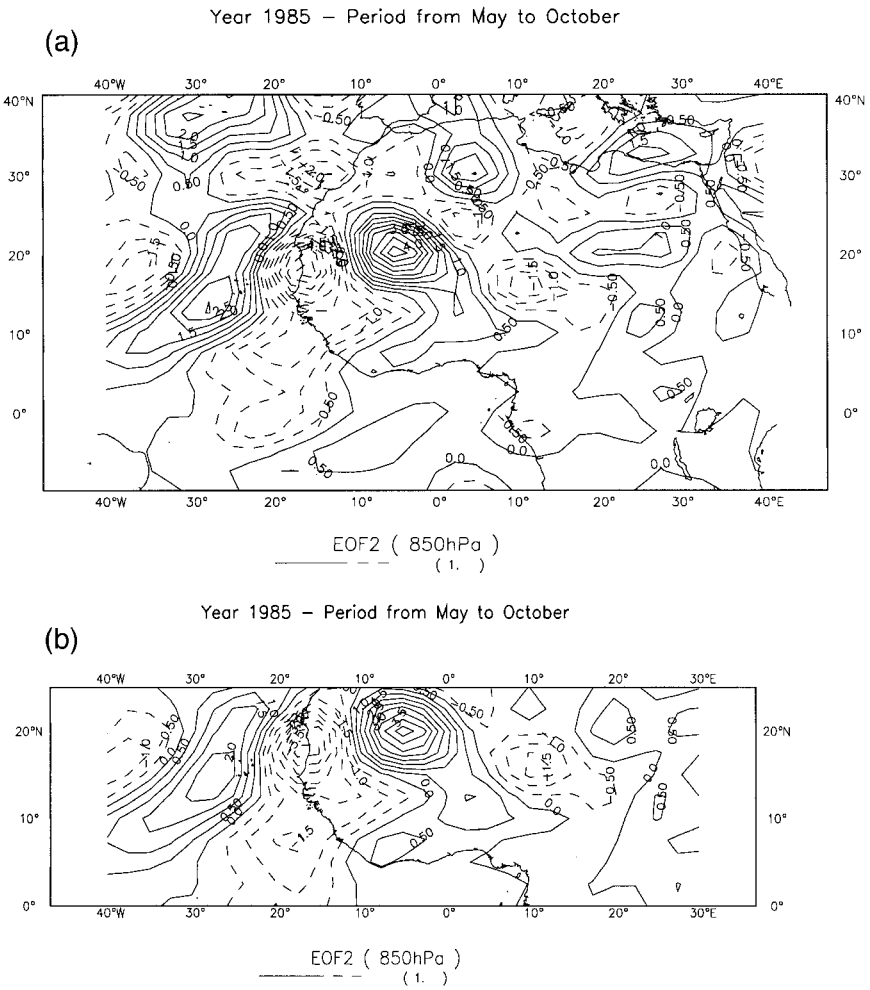

FIG. 4. Pattern of the second eigenvectors of the filtered vorticity at 850 hPa from the ECMWF analyses for the May–Oct period and the year 1985; (a) EOF analysis computed on the STSA domain, (b) EOF analysis computed on the CEOF domain.

ysis and simulation, though with a tendency to have larger periods in the simulation. AEWs are thus slower in the model; this kind of behavior has already been noticed by several authors (e.g., Reed et al. 1988b; Druyan and Hall 1994). It seems possible that, because of the rather low resolution of the GCM (T42), the shear of the AEJ is too weak compared to the reality; and, as a consequence of a weaker shear (in the framework of energy exchange between the wave and the jet), the waves tend to propagate more slowly, as shown by Paradis et al. (1995).

Figure 7 shows the two-dimensional space spectra of the westward traveling waves (ECMWF above, GCM below, for 1985) in the time domain of the AEWs (summation of the power density over the 3–5 day window, here also expressed in thousandths of the total variance of this diagram), with the meridional (zonal) wavenumbers in the abscissa (ordinate). Thus, there is evidence for a predominance of west-northwest propagation because of larger variance for negative meridional wavenumbers. However, the propagation of the simulated AEWs is more zonal due to the existence of a more symmetrical pattern of variance (along the abscissa) on the GCM spectrum.

By computing the variance in the AEW space–time spectral window (as mentioned earlier), we were able to compare the space–time variability coming from the analysis versus the simulation for all the years. The discussion of these results will be presented in the next section, insofar as the CEOFA gave complementary and more precise results on these aspects.

b. Intraseasonal variability

In order to address this topic, we have computed, at each grid point of our space domain and for each month from May to October (of each year), the time variance for westward traveling oscillations in the AEW space–

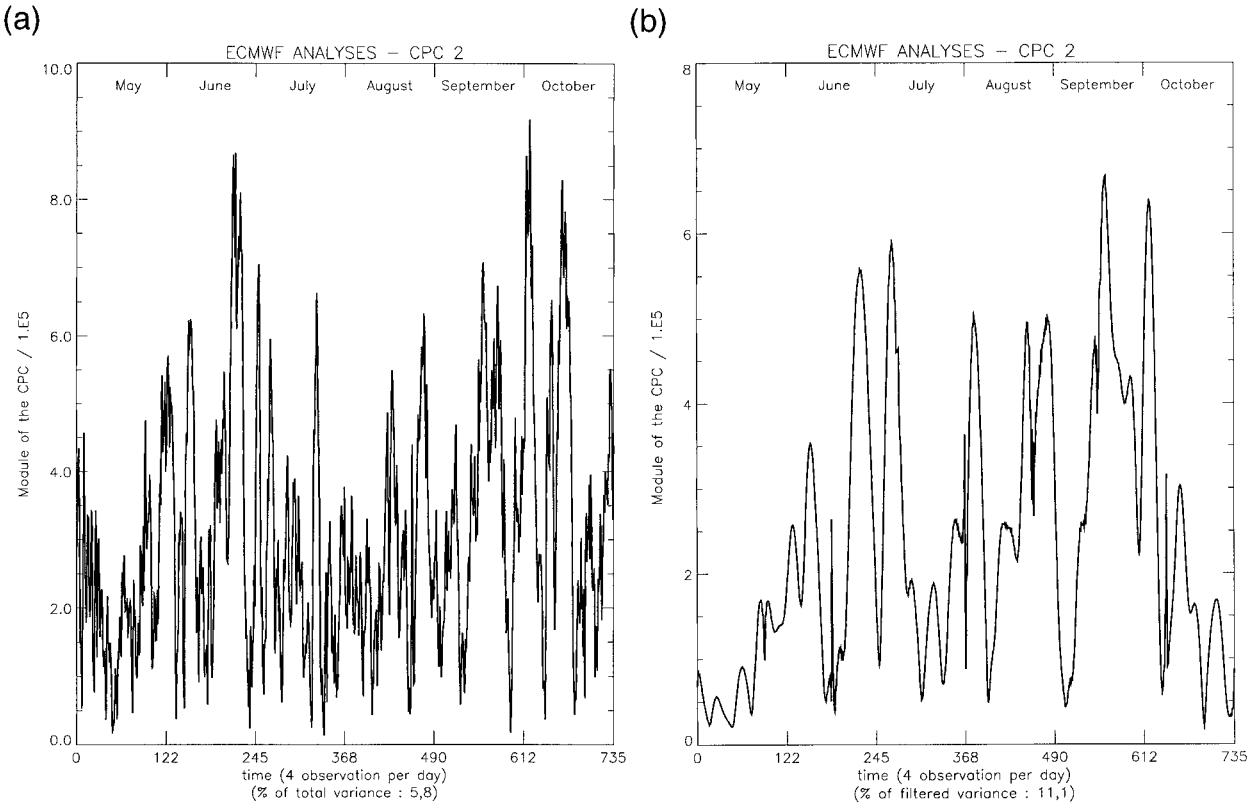

FIG. 5. Time series of the module of the second CPC of vorticity at 850 hPa (s^{-1}) from the ECMWF analyses for the May–Oct period (four observations per day on *x* axis) and year 1985; (a) raw data, (b) filtered data.

time spectral window, which we determined in the previous section (following Hayashi 1979). The AEWs are then treated as wave packets consisting of multiple wavenumbers. It is worthwhile to notice that the wave packet treatment could also enable the calculation of group velocities and envelope time spectra at each grid point. Figure 8 shows the contour of this relative vorticity time variance in June, July, August, and September 1985 (Figs. 8a–d for ECMWF and Figs. 8e–h for the GCM). The location of variance maxima gives a good idea of the wave tracks. There is a qualitative agreement between the simulation and the analysis in terms of the seasonal evolution of the location and intensity of the variance maximum. Indeed, the largest variance occurs generally in August; moreover, the variance maximum located at the edge of West Africa in July and August moves southwestward over the ocean in September. During the month of June, the variance is located generally over land but in the south, compared to the July and August cases; in June 1985, the wave variance was weak in the analysis and even weaker in the simulation. One has to be quite cautious about the significance of this comparison. Indeed there are only about eight AEWs per month; moreover, as the GCM simulation was not a month forecast, one cannot expect to quantitatively measure the distance between the analyzed and simulated variance patterns. Nevertheless, we have found the same overall resemblance in the seasonal evolution between the simulation and the analysis for the other years (not shown).

However, there are discrepancies between the model and the analysis. The most important failure is the following. The simulated variance maximum is more zonal and more constricted in latitude than the analyzed. More precisely, the simulation gives generally one track (one main maximum of variance, see Figs. 8f,g), which is located between two prefered tracks produced by the ECMWF analyses. These two tracks, one around 10°N and another one around 20°N (with a much larger variance intensity), especially in July and August (see Figs. 8b,c), have already been noted by several authors (e.g., Reed et al. 1988b). At this stage, it is difficult to adequately explain this discrepancy. At least a large part of the northward shift of the simulated AEJ (not shown) appears to be mainly due to the fact that the surface processes are not properly reproduced in the model (as previously mentioned); the albedo is especially too small over the Sahel, which tends to produce more precipitation (because of the increased evaporation) and therefore tends to shift the meridional temperature gradient northward, in association with the AEJ. This phenomenon could be enhanced through a positive feedback mechanism between the precipitation and the AEJ latitudinal location. This northward shift of the simulated

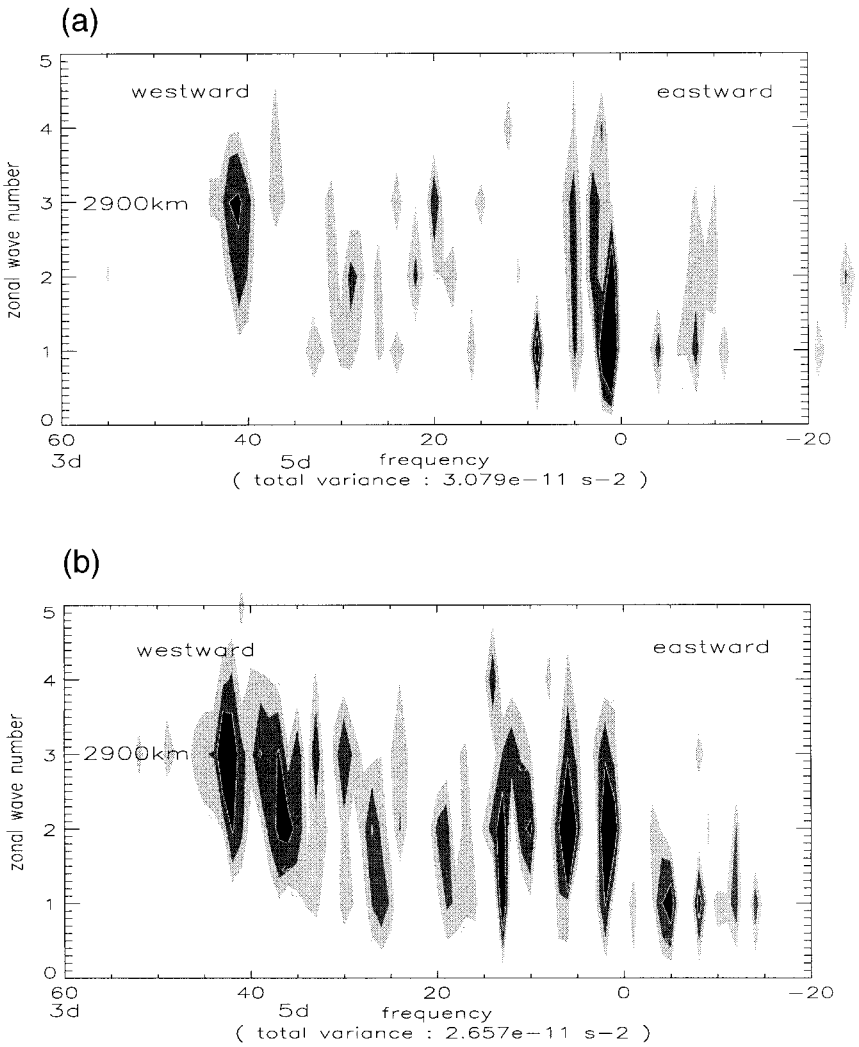

FIG. 6. Space–time spectra for the relative vorticity at 850 hPa (traveling waves only) from May to Oct 1985, expressed in thousandth of the total variance (isolines: 2, 3, 8); (a) ECMWF, (b) CNRM GCM. Abscissa are given in time harmonics (maximum period of 184 days, negative for eastward propagation), ordinate in zonal harmonics (maximum wavelength of 8800 km).

AEJ may explain the fact that the simulation gives less variance south of 12°N compared to the analysis.

On the other hand, another major discrepancy between the simulation and the analysis is the fact that there is more variance east of 10°E in the model, as also indicated by Druyan and Hall (1994). At this stage, it is difficult to explain this discrepancy. There is a lack of observations in this region, therefore the analysis might not be reliable.

c. Energetics

Zonal wind–meridional wind (u, v) and meridional wind–temperature (v, T) covariances at 850 hPa have been computed in the AEW space–time spectral window, with the help of a space–time cross-spectrum calculation (Hayashi 1982). Figure 9 shows these covariance contours at 850 hPa, in July 1985 [(u, v) for ECMWF and the GCM, and (v, T) for the GCM]. It would have been more relevant to consider the 700-hPa level, the closest to the AEJ level, to compute the (u, v) covariance, but the simulated data were not available at this level. Nevertheless, we notice a close correspondence between the simulated and analyzed (u, v) covariance. A zone of positive (u, v) values lies south of the AEJ (zone in which $\partial u/\partial y$ is negative) in the western part of Africa, meaning a contribution to a barotropic transfer of kinetic energy from the jet to the waves. Furthermore, there is a zone of negative (v, T) values lying around the location of the AEJ (zone in which $\partial T/\partial y$ is positive), meaning a contribution to a baroclinic transfer of potential energy from the jet to the waves over that region (between 12° and 18°N, rather to east of the region associated with the barotropic transfer of kinetic energy). This pattern is very close to the one obtained by Reed et

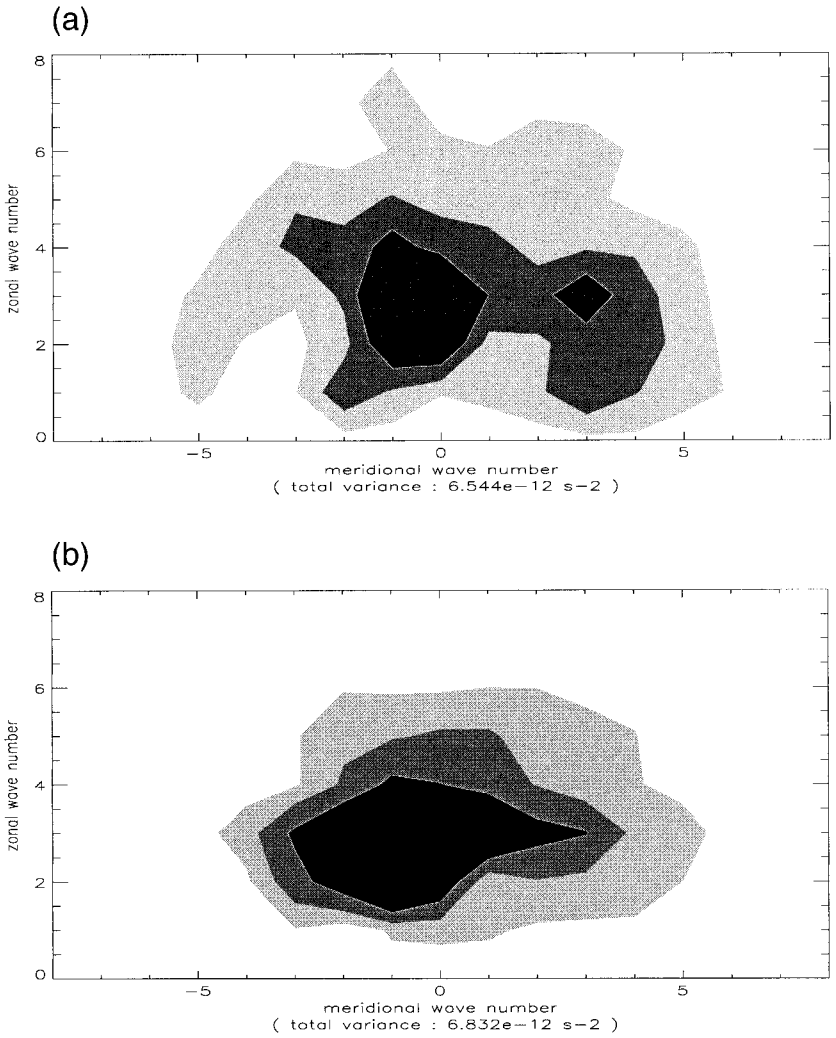

FIG. 7. Space spectra for the relative vorticity at 850 hPa (westward traveling waves only over the 3–5-day time window) from May to Oct 1985, expressed in thousandth of the total variance (isolines: 10, 20, 30); (a) ECMWF, (b) CNRM GCM. Abscissa are given in meridional harmonics (maximum wavelength of 5500 km, negative for southwestward propagation), ordinate in zonal harmonics (maximum wavelength of 8800 km).

al. (1988b) with the ECMWF data for August–September 1985. Generally identical results have been noticed for the other months in terms of the location of the region of barotropic and baroclinic energy transfer versus the AEJ location. Therefore, it seems that baroclinic transfer is predominant at the beginning of the wave life cycle and that barotropic transfer becomes important over the western part of the continent [as already noticed by Norquist et al. (1977) and Albignat and Reed (1980)]. This conclusion is also valid for the simulated AEWs.

4. Results from complex empirical orthogonal functions analysis

We have to remember here that all results discussed in this section have been obtained in a year-by-year analysis using a 6-month period (namely, from May to October). We chose to perform a year-by-year analysis because there is no evidence (particularly looking at the location of the InterTropical Convergence Zone (ITCZ) and the AEJ) that AEWs should have the same track location each year. Thus, a global analysis could give ''averaged'' patterns that could induce incorrect interpretation because of the suspected interannual variability of the AEW tracks. As discussed in section 2b, results from raw and filtered data are quite similar. Filtered data just make the signal clearer, and the results are easier to interpret. Therefore, we present only the results obtained with filtered data. In section 4a, we mainly discuss the results of CEOF analysis for the year 1985 to compare and validate our conclusions with the comprehensive synoptic study done by Reed et al. (1988a)

for this year. The interpretation of the CEOF patterns and time series is quite similar for the other years, and we attempt to bring out the nature of the interannual variability by considering the other years in section 4b.

a. Patterns of CEOFs and time series of CPCs

The main result of the CEOFA is the partition of the vorticity space–time variability at 850 hPa into two main and complementary modes of variability. We selected these two modes because they always appear in first or second position in terms of percentage of variance. They also represent the modes that can be provided a reasonable interpretation and are also seen to be quite ''stable'' in the year-by-year analysis. We will discuss these two points in more detail in this and subsequent sections. At this stage, it may be noted that we named these modes respectively mode 1 and mode 2 without any consideration to their rank (first or second in term of percentage of variance), which depends on the considered year as shown in the next section.

The percentage of the total variance (i.e., variance of the raw data) of CPCs associated with these patterns range from 3% up to 11%, depending on the year and the rank of the CPC.

The pattern of the CEOF associated with mode 1 for the ECMWF analyses is shown in Fig. 10a. The module of the CEOF exibits a maximum of space amplitude located between 15° and 20°N over the continent, west of the Greenwich meridian. Then, the axis of the maximum of space amplitude curves southward over the Atlantic Ocean, and the space amplitude decreases toward the western part of the domain. This mode has been called ''northern single-track'' mode. The time phase of the associated CPC (namely, CPC1, not shown here) is very regular, representing a quasi-constant period of the waves in the range of 4–5 days. The space phase is well organized over regions with large values of the CEOF module. The space phase gradients associated with the previous period give phase speeds ranging from 6 up to 8 m s^{-1} and westward propagation along the axis of the maximum of variance (which is identical to the space amplitude maximum).

The second mode is complementary to the first one in the space–time domain. Its main feature looks like a ''dual-track'' pattern and is shown for the ECMWF analyses in Fig. 10b. The primary maximum of space amplitude is located on the extreme north of the area (between 18° and 25°N over the western part of the continent), and a secondary maximum can be seen over the Atlantic Ocean, centered near 10°N. When this mode has a large variance (e.g., in 1988), the secondary maximum seems to extend over the continent, notably along the coast of the Gulf of Guinea. The space phase, well organized over the regions of maximum space amplitudes, gives zonal AEW propagations over the northern part of the domain and a slight curvature toward the north for the southern part. The periods of CPC associated with this mode (namely, CPC2) are shorter than for mode 1, around or less than 4 days. This gives phase speeds roughly in the range of 6–8 m s^{-1}, which are the same as for the previous mode. Interestingly, mode 2 has larger values of variance over the Atlantic Ocean than over land for the southern cell of the mode; this is quite consistent with known properties of AEWs observed in the southern part of West Africa (Reed et al. 1988b).

It is essential to discuss the reality of the two modes, in view of interpretation problems of empirical modes obtained by the use of factorial methods. For this purpose, we studied two idealized waves, slightly to fully mixed in space on the same kind of domain and with the same characteristics as AEWs (i.e., wavelength around 3000 km and period around 4 days with a 6-h lag between the two periods). We can summarize the results as follows: the quality of the representation of the modes depends mainly on the mixing of the patterns and, in all cases, periods are correctly estimated. These results are consistent with theoretical or observational studies using CEOFA (Horel 1984; Bloomfield and Davis 1994) and with Fourier function properties. Insofar as our modes are quite well spatially separated (except for the year 1987), we can consider that patterns are detected with a low distortion. Additionally, we compared the space representation of the time variance from STSA and from the two added modes of CEOFA. The patterns shown in Figs. 11a and 11b highlight, qualitatively, a good agreement between the two methods for 1985. This agreement has also been noticed in the other years. Finally, concerning the physical distinction between the two modes, one can argue by comparing results from CEOFA and the two components of AEW already presented in section 1. As discussed earlier, we have two components for AEW giving two vorticity tracks at 850 hPa (roughly one near 18°N and the other near 8°N). Schematically, the first one corresponds to large vorticity centers located in the north of the domain where dry conditions predominate, while the second one corresponds to the southern vorticity centers where moist convection is able to interact with it. Concurrently, the latitudinal location of the southern variance of mode 2 is the closest to the precipitation maximum. Additionally, the synoptic study done by Reed et al. (1988a), using a day-by-day tracking of AEWs for 1985, gives an interesting point of comparison. The AEW tracks estimated by the synoptic analysis are quite similar to those given by the maximum of variance of the two modes exibited by CEOFA. Moreover, the CPC maxima are located (in time) close to the date given by the synoptic analysis, and the partition between modes 1 and 2 seems to correspond well to double or southerly tracks (for mode 2) and to northerly curved tracks (for mode 1) of the synoptic analysis. Of course, the synoptic study does not make any partition between the AEWs; but, finally, the relationship that seems to exist between the interannual variability of mode 2 and the rainfall

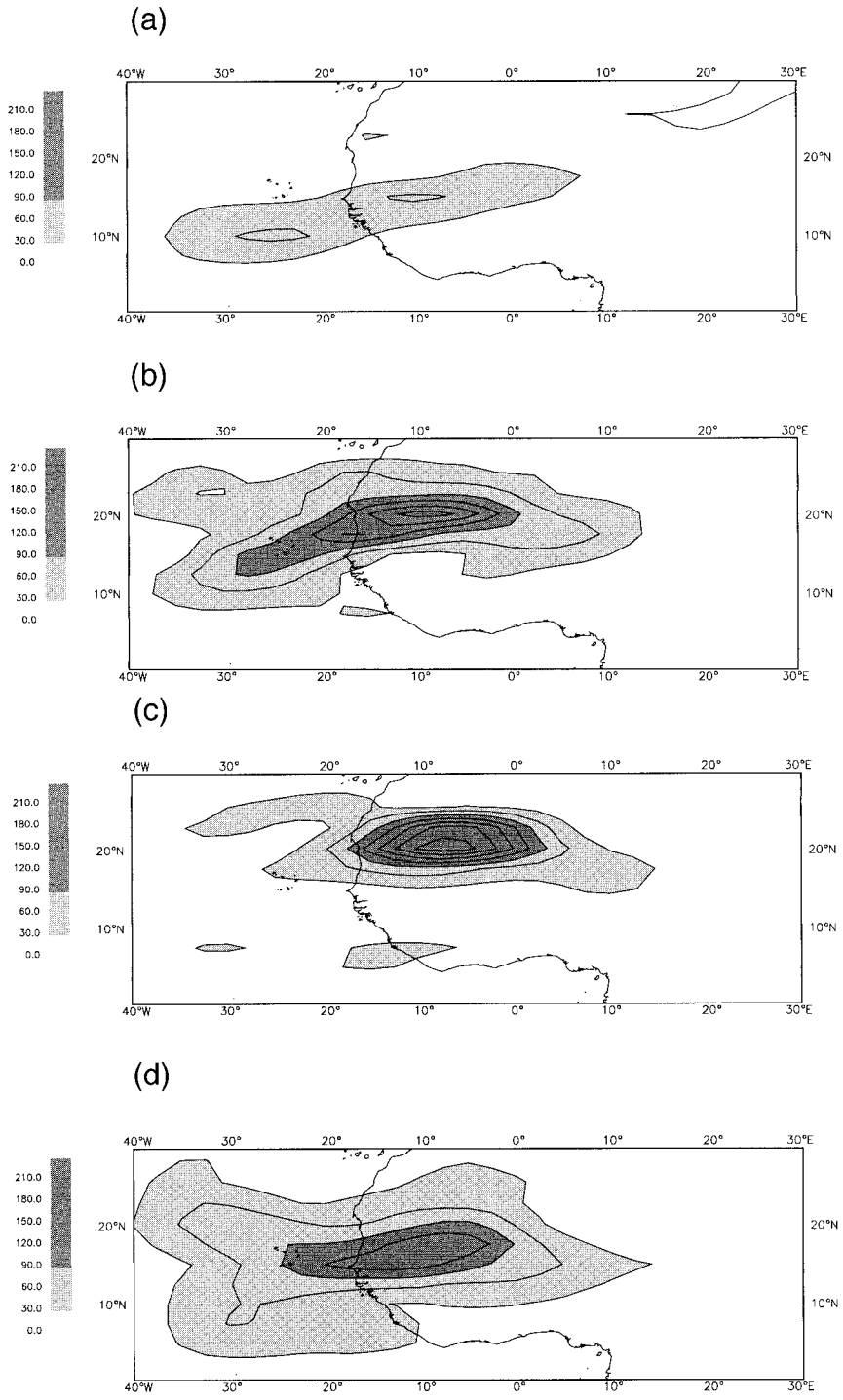

FIG. 8. Relative vorticity time variance (in s^{-2}) in the AEW space–time spectral window, for traveling waves only; (a) ECMWF Jun 1985, (b) ECMWF Jul 1985, (c) ECMWF Aug 1985, (d) ECMWF Sep 1985, (e) CNRM GCM Jun 1985, (f) CNRM GCM Jul 1985, (e) CNRM GCM Aug 1985, (f) CNRM GCM Sep 1985. Contour interval is 3×10^{-11} s^{-2}.

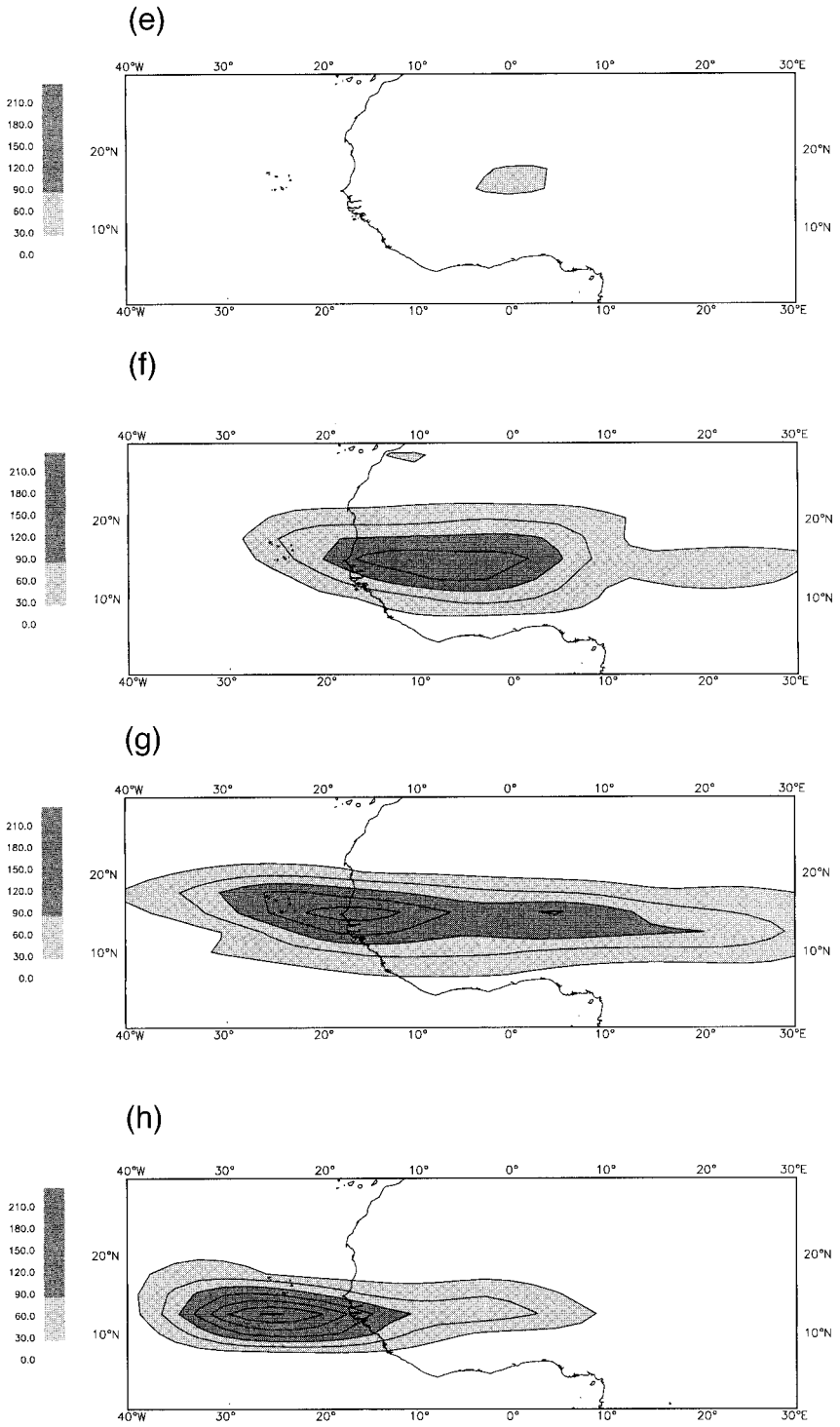

FIG. 8. (*Continued*)

over West Africa (see next section) strengthens the following interpretation: the northern single-track mode (i.e., mode 1) should be preferentially representative for AEWs associated with dynamical effects (i.e., with a predominant northerly component), while the dual-track mode (i.e., mode 2) should catch the majority (in comparison with mode 1) of the AEWs associated with diabatic effects. In other words, the dual-track mode composes the majority of the AEWs characterized by a significant southerly component but also some AEWs char-

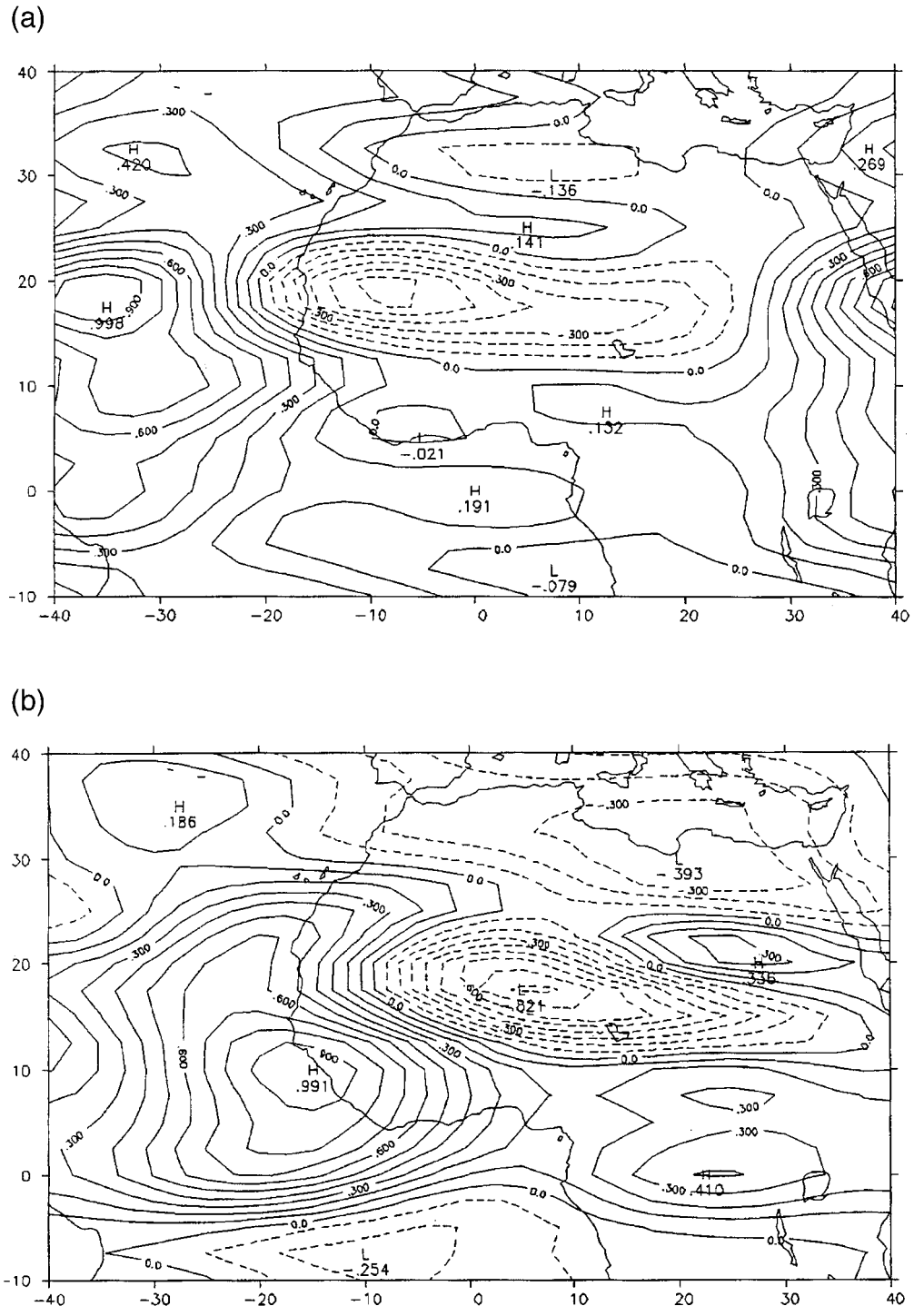

FIG. 9. Time covariance of meteorological fields at 850 hPa, filtered in the AEW space–time spectral window for Jul 1985; (a) (u, v) from the ECMWF (10^{-1} m^2 s^{-2}), (b) (u, v) from the CNRM GCM (10^{-1} m^2 s^{-2}), (c) (v, T) from the CNRM GCM (10^{-1} K m s^{-1}).

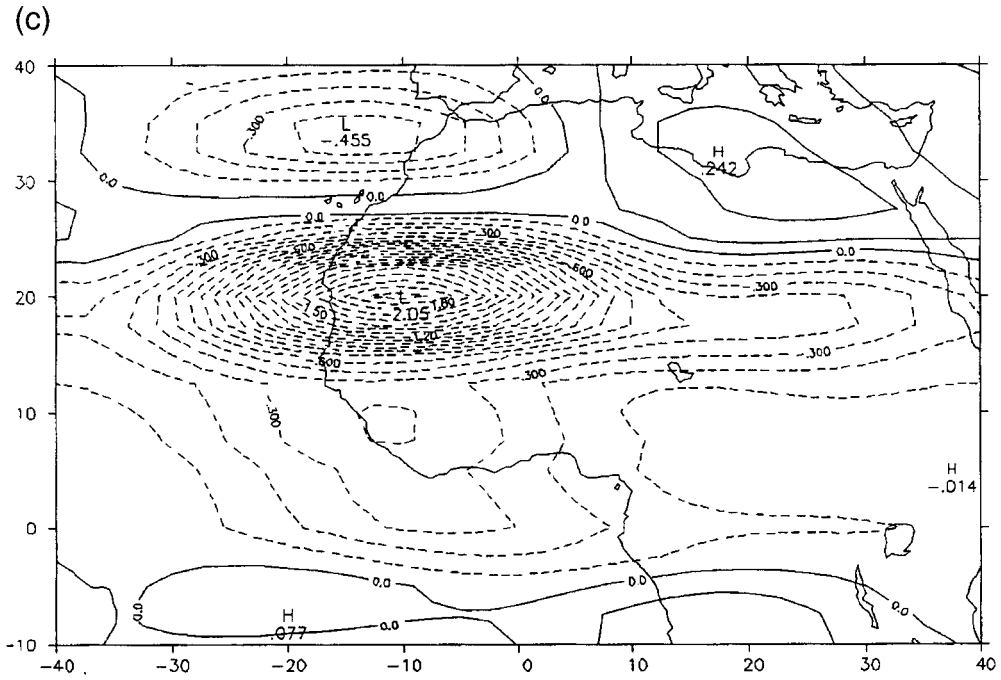

FIG. 9. (*Continued*)

acterized by an intense northerly component (located around 20°N). The northerly component should grow on the northern side of the AEJ, while the southerly component should grow on its southern side and thus interacts with the deep convection, as was previously discussed in the introduction. However, it is only a statistical study and not an individual tracking, so at this stage, we wish to caution that it is possible to have some confusing features picked up by the two modes.

In the AMIP run, the pattern of the module of mode 1 (Fig. 12a) is shifted toward the south (below 15°N) and shows a quasi-zonal pattern without any curvature over the Atlantic Ocean. The time phase exhibits, generally, a greater period than the one from the ECMWF analyses, and phase speeds seem to be slower than those discussed in section 3a. However, we have to be cautious with the phase speed because, looking at analytical waves in order to evaluate the CEOFA, we have seen that the space phase is one of the most sensitive parameters to sampling problems. Consequently, we must have less confidence in its estimation (through the method) compared to that of the other parameters (module of CEOF, of CPC, and period), despite the fact that we tested different estimation methods for the space-phase gradient.

For mode 2 of the GCM (Fig. 12b), one can also notice a dipole pattern that is quite similar to the one of the ECMWF analyses. However, one can notice a geographical shift for the maxima, southward for the northern one and northward for the southern one. This gives a global pattern that is more centered on 15°N. The associated space phase gives quasi-zonal propagations over all the main regions. The periods of the waves are generally greater than for the ECMWF analyses, and consequently, as discussed in section 3a and for the mode 1, the phase speeds are slower in the GCM. It may be noted that the lack of agreement in the space representation of the southern track pointed out in the GCM is consistent with the northward shift of rainfall in the GCM (see section 2a). This is linked to the rather good relationship between rainfall and vorticity propagations in the GCM.

Here, we must underline that the interpretation of the two modes of the model is less clear than that for the ECMWF analyses. The space discrepancies of the GCM should be notably related to its bias in the location of the AEJ, as already mentioned in section 3b. Another difference that can be noted between the analyses and the GCM is that there are local maxima in the eastern part of the GCM CEOFs that do not really exist in those of the ECMWF. It is difficult to interpret this difference because of the lack of observational data (see discussion in section 3b).

The time series of CPC1 are shown in Fig. 13a for the ECMWF analyses and in Fig. 13b for the GCM dataset. The main characteristics of the two curves are a seasonal modulation of the time amplitude of the waves and a low-frequency modulation in the 20–60-day bandwidth. These cycles are statistically significant both in the ECMWF analyses and the GCM dataset (5% level with reference to ''red noise''; Jenkins and Watts 1968). Comparing Figs. 13a and 13b, one can see that the low-frequency modulation is only qualitatively duplicated by the GCM. One can particularly notice a

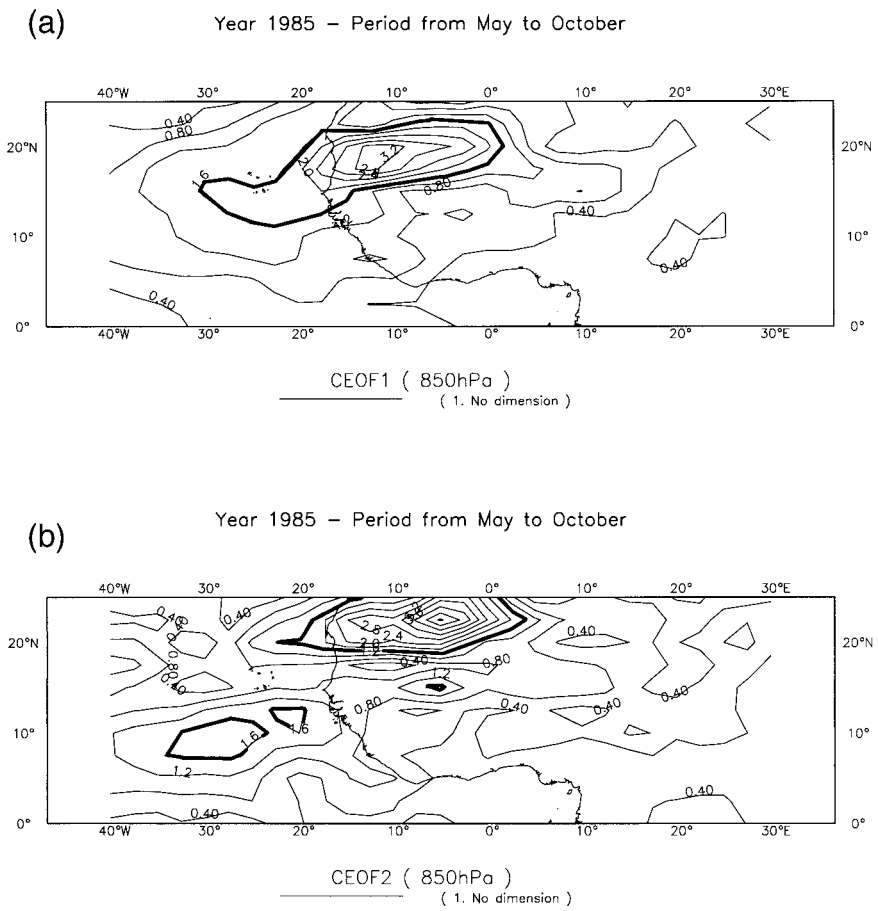

FIG. 10. Module of the first CEOFs of filtered vorticity at 850 hPa for the ECMWF analyses and the year 1985; (a) mode 1, (b) mode 2. Contours from 1.6 indicate regions with significant values of variance.

phase shift due to a late start of the model more clearly illustrated in the next section (see projection of AMIP dataset on eigenvectors of the ECMWF analyses). The same kind of behavior can be noticed for CPC2 (not shown here), in both the ECMWF analyses and the GCM dataset. The main difference between CPC1 and CPC2 is the period of the low-frequency modulation, which is generally greater for CPC1 (maximum of modulation in the range of 40–50 days) than for CPC2 (maximum of modulation in the range of 20–40 days). One can notice that the low-frequency modulation is not caused by the sampling method used to compute the cross-spectrum matrix (see section 2b) because it exists in the time series of the PCs (e.g., see Fig. 16a), which are performed using all the observations. Moreover, the three periods of AEW activity separated by clear breaks (indicated by arrows in Fig. 13a) show that the modulation of the signal is not a shapeless seasonal cycle but a real low-frequency modulated signal.

Thus, generally speaking, the above results exhibit a very important point for extended-range forecasts and future developments. Druyan and Hall (1994) showed spectra of meridional wind at 890 and 780 hPa with significant power in a 2–4-week bandwith using 32-day time series of a GCM dataset. In section 3a, we have also shown spectra with power in the 30–50-day period range. The major point that emerges here is that the AEW activity is modulated by a low-frequency mode. In the near future, we will have to determine what kind of physical or dynamical processes are involved in this modulation. As preliminary hypotheses, we can propose three directions for further development. First, one can consider dynamical interactions between the divergence in altitude and the AEW. Divergence in the high troposphere could favor vertical developments of convection and therefore interact with AEW. In this way, we could quote the role of the eastward moving Madden–Julian oscillation (MJO). We can also suggest that the divergence in altitude over West Africa could be influenced by Tropical Easterly Jet (TEJ; Hastenrath 1991), which is notably linked to the Indian summer monsoon. So breaks and active periods of the Indian monsoon being modulated on a low-frequency range could be linked to the low-frequency modulation shown above.

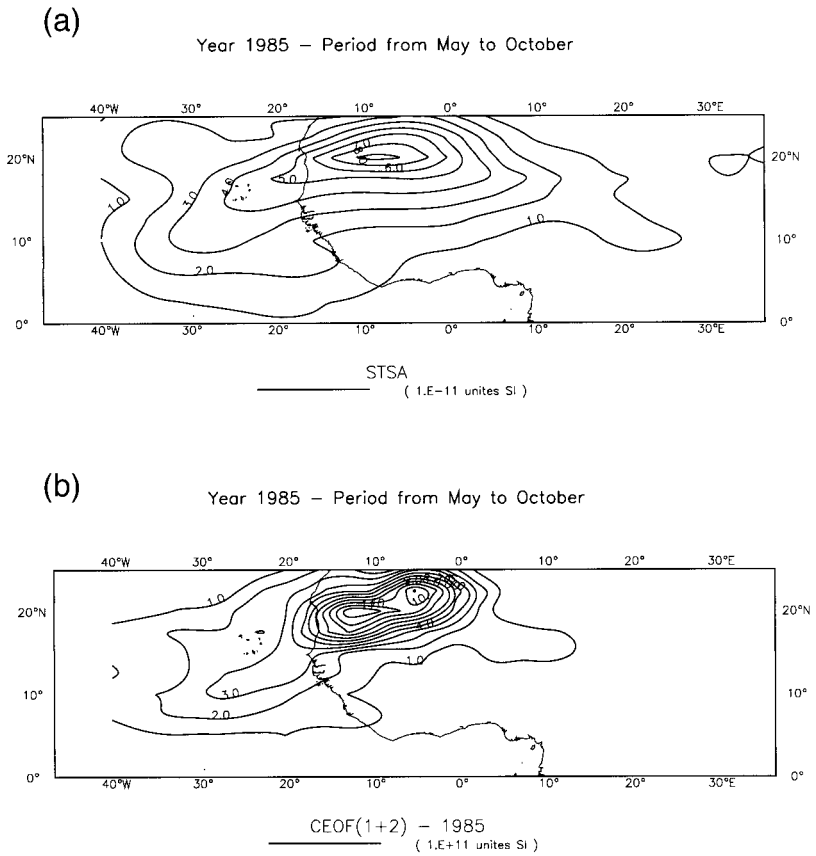

FIG. 11. Space representation of the time variance (s^{-2}) for the year 1985 from the ECMWF analyses; (a) the STSA method, (b) the two first modes of the CEOF analysis. Contour interval is 10^{-11} s^{-2}.

A preliminary study of MJO in the CNRM GCM indicates that the maximum of AEW activity occurs during periods of divergence anomalies at 200 hPa over West Africa. Second, one may consider land–atmosphere feedback mechanisms. Preliminary studies in this direction (Céron and Guérémy 1994) seem to indicate that the maintenance of dry surface conditions over the Sahelian region inhibits the westward propagation of AEWs in the GCM. Third, it may be conjectured that the presence of two modes with quite comparable periods could produce pulsations in the vorticity field. However, the clear separation between the two modes leads us to doubt the validity of this hypothesis.

b. Interannual variability

Looking at the total variance of the vorticity field (see Table 1), one can notice, in the ECMWF analyses, that the last two years show larger values, while the earlier five show rather low values. In the GCM, the contrast between low and high values is less clear than in the analyses, but we can consider that the AMIP simulation exibits a reasonable part of the total variance, except for 1983, which is the worst simulated year, while 1982, 1986, and 1988 are well simulated. There appears to be no particular behavior in the ECMWF variances that could be linked to changes in the analyses (see discussion in section 2). The percentage of the total variance (i.e., variance of the raw data) that could correspond to AEWs (i.e., associated with patterns and periods in the range of wavelengths and periods of AEWs) oscillates between 7% and 15% depending on the year (STSA gives quite similar results).

For filtered data (see Table 1) the ECMWF variances represent a quasi-constant part of 25% of the total variance (i.e., variance of the raw data), while GCM variances represent less percentage (around 22%) and have a greater variability (from 18% up to 27%). Accordingly, one can remark that, except for 1988, the filtered vorticity variance is less well simulated than the total vorticity variance. This could be linked to some failures of the spectral representation of the GCM, which produces relatively too much variance in the low-frequency domain and less variance in the high-frequency domain, as one can see from spectral analysis (see discussion in section 3a). However, the conclusions are roughly the same for both the analyses.

Looking at the interannual variability of the two main

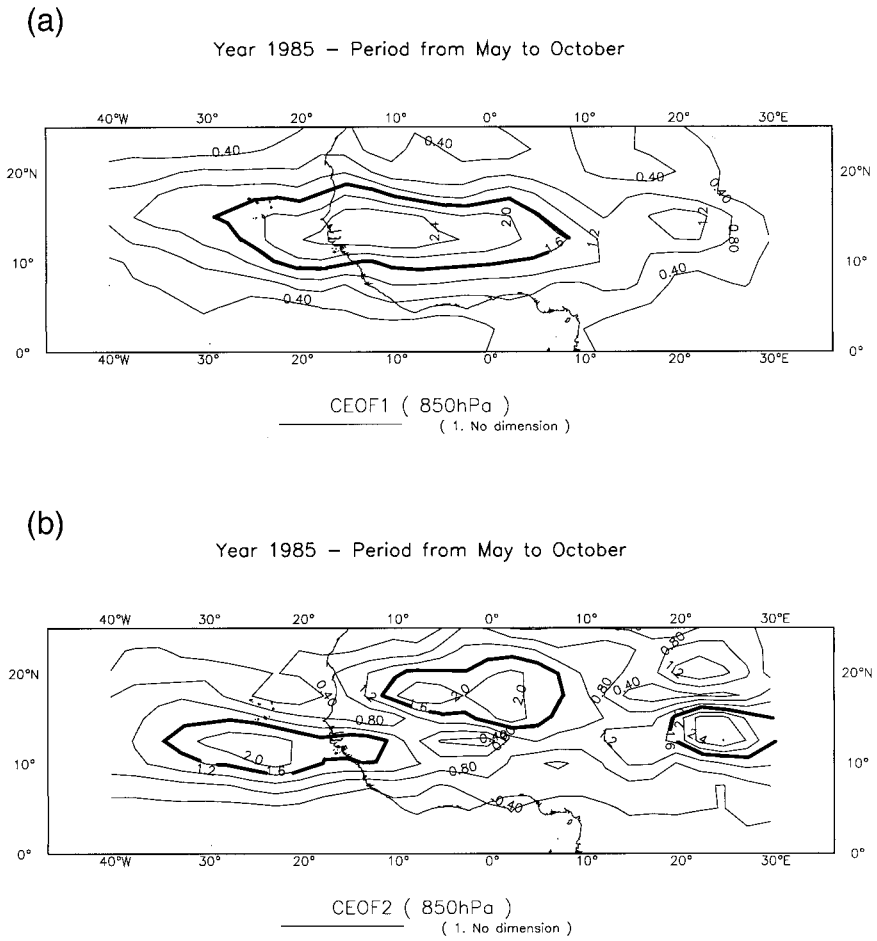

FIG. 12. Module of the first CEOFs of filtered vorticity at 850 hPa for the CNRM GCM and the year 1985; (a) mode 1, (b) mode 2. Contours from 1.6 indicate regions with significant values of variance.

modes brought out by CEOFA, it may be noted (in Table 2) that the GCM gives a rather good description of the added variance of the two modes (except for 1983) and preserves the contrast between high (1985, 1988), low (1982, 1983), and intermediate variances. Years 1982, 1987, and 1988 seem to be very well simulated without any consideration of space discrepancies.

Detailing each mode and generally speaking, the GCM provides slightly less variance than the analyses. One can see that the simulated variance for each mode is worse (compared to the analyses) than the added variance of the two modes previously discussed. This indicates that the total variance for the two modes is quite correct when the distribution of the variance between the two modes is not very well reproduced. However, the main difference for the mode 2, between 1988 and the other years, is well duplicated by the GCM; and the three years with the lowest variance for mode 1 are also detected by the model (but not in the same order).

At this stage, we can highlight the behavior of the two modes regarding the interannual variability of the rainfall over West Africa. During the period of study, 1988 was the only year with a rather good amount of precipitation (e.g., Fig. 2 from Lare and Nicholson 1994). Also, it was the only year where mode 2 was predominant. This is probably linked to the fact that, as discussed in the introduction, the southerly tracks (related to mode 2) correspond to the AEWs that are the most related to rainfall; the squall lines are indeed mainly observed in the southern part of the domain (Desbois et al. 1988). And finally, it is very gratifying to observe that the GCM was able to reproduce very well the variance seesaw of the two modes between 1988 and the other years.

Looking at ECMWF analysis periods (see Table 3), one can see that the periods of mode 1 are roughly larger than 4 days (averaged period around 100 h) and those of mode 2 are less than 4 days (averaged period around 95 h). This may be connected to the previous behavior of the two modes; we can particularly point out that 1988 is the only year that has short periods and high variance for mode 2. Of course, the difference between

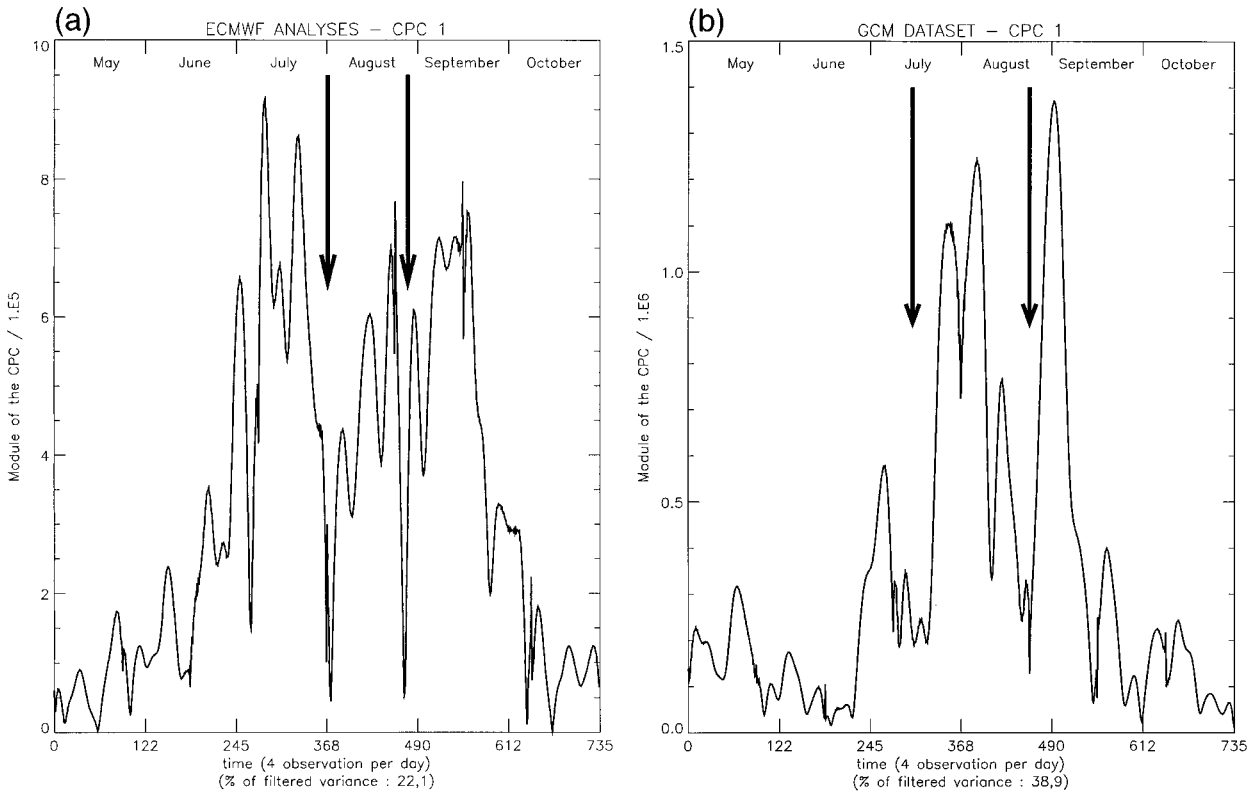

FIG. 13. Time series of the module of the first CPC of filtered vorticity at 850 hPa (s^{-1}) for the year 1985; (a) ECMWF, (b) CNRM GCM. Arrows indicate the low-activity phase.

the periods is not necessarily significant. However, this can be related, on one hand, to the positive correlation between the amplitude of AEWs and the mean size of cloud clusters (Toledo Machado et al. 1993) and, on the other hand, to the fact that AEWs with a period shorter than 4 days seem to be more efficient for rainfall than those with a period greater than 4 days (Saloum 1993). These later features seem to characterize a wet year.

The AMIP periods (see Table 3) show that the model has a clear tendency to produce waves with a greater period than the analysis. This is particularly sensitive for mode 2, which seems to be the closest to rainfall. So it appears that the most interesting mode for rainfall purpose is, generally speaking, the worst simulated mode.

Finally, looking at patterns of the time variance for four years of the chosen period, we can point out some interesting findings. For the ECMWF analyses, the pattern of the two modes (see Figs. 14a and 15a) shows a good geographical stability in the latitudinal location of the maxima of variance with, obviously, an extension of the cells depending on the variance in each mode (see discussion above) and a longitudinal location variability of the maxima of variance. Looking at Table 4, one can see that this geographical stability is good for all the years except for mode 2 in 1982 and for the two modes in 1987. However, for this last year, looking at the tracks of corresponding AEWs, this is consistent with the fact that, during 1987, the ITCZ had an abnormal location (more to the south than normal), and

TABLE 1. Vorticity variances (10^{-10} s^{-2}) corresponding to the different years.

Year	1982	1983	1984	1985	1986	1987	1988
ECMWF raw data	1.368	1.405	1.437	1.365	1.405	1.793	1.766
AMIP raw data	1.175	0.932	1.021	1.135	1.305	1.344	1.487
ECMWF filtered	0.317	0.345	0.370	0.372	0.359	0.448	0.443
AMIP filtered	0.211	0.172	0.236	0.297	0.236	0.349	0.406

TABLE 2. Variances (10^{-11} s^{-2}) of ECMWF modes and GCM modes corresponding to the different years.

Year	1982	1983	1984	1985	1986	1987	1988
ECMWF Mode 1	0.45	0.53	0.81	0.82	0.74	0.61	0.40
ECMWF Mode 2	0.24	0.36	0.33	0.41	0.31	0.47	0.82
AMIP Mode 1	0.35	0.31	0.64	1.12	0.45	0.65	0.42
AMIP Mode 2	0.20	0.19	0.16	0.33	0.23	0.36	0.88

TABLE 3. Periods (days) of ECMWF modes and GCM modes for the different years.

Year	1982	1983	1984	1985	1986	1987	1988
ECMWF Mode 1	3.9	4.1	4.3	4.1	4.2	4.3	4.0
ECMWF Mode 2	4.0	3.8	4.0	3.8	4.1	3.9	3.9
AMIP Mode 1	4.2	4.1	4.1	4.9	4.4	4.6	4.6
AMIP Mode 2	4.5	4.3	4.2	4.7	4.9	4.0	3.8

this year was dry, except over the western part of Africa (particularly over Senegal).

For the AMIP run (see Figs. 14b and 15b), one can remark that the variance pattern is not very good for mode 1 and even worse for mode 2. As discussed earlier, the maxima of variance are not correctly located (see Table 4). So it appears that the mode that seems the closest to the rainfall has the worst representation in the model. Further, the GCM provides roughly the same location of tracks for AEWs and therefore is not able to simulate the pattern of the AEW variability correctly for atypical years such as 1987.

c. *Projection of the GCM dataset on the eigenvectors of the ECMWF analyses*

We cannot compare very easily time series obtained from the analyses and the GCM because the empirical functions are not the same. In order to have a better comparison between the times series, we have used a common base given by our reference. Consequently, we projected the GCM dataset on the first 20 eigenvectors obtained from the ECMWF analyses (which preserve a large percentage of variance and give easier calculations instead of keeping all eigenvectors). Then, we recomputed traveling waves using the CEOFA.

The comparison between time series of principal components of the ECMWF data and the projected AMIP

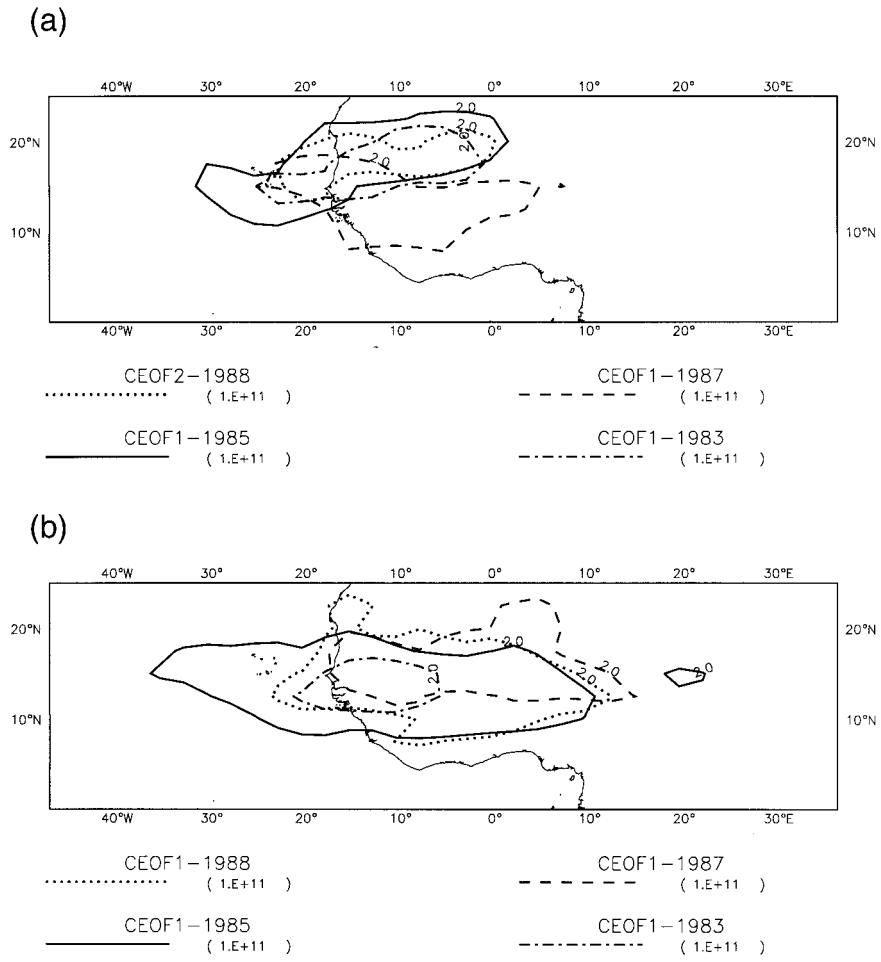

FIG. 14. Schematic space representation of the time variance for the years 1983, 1985, 1987, and 1988 for the mode 1 of filtered vorticity at 850 hPa; (a) ECMWF, (b) CNRM GCM. Contour interval is 2×10^{-11} s^{-2}.

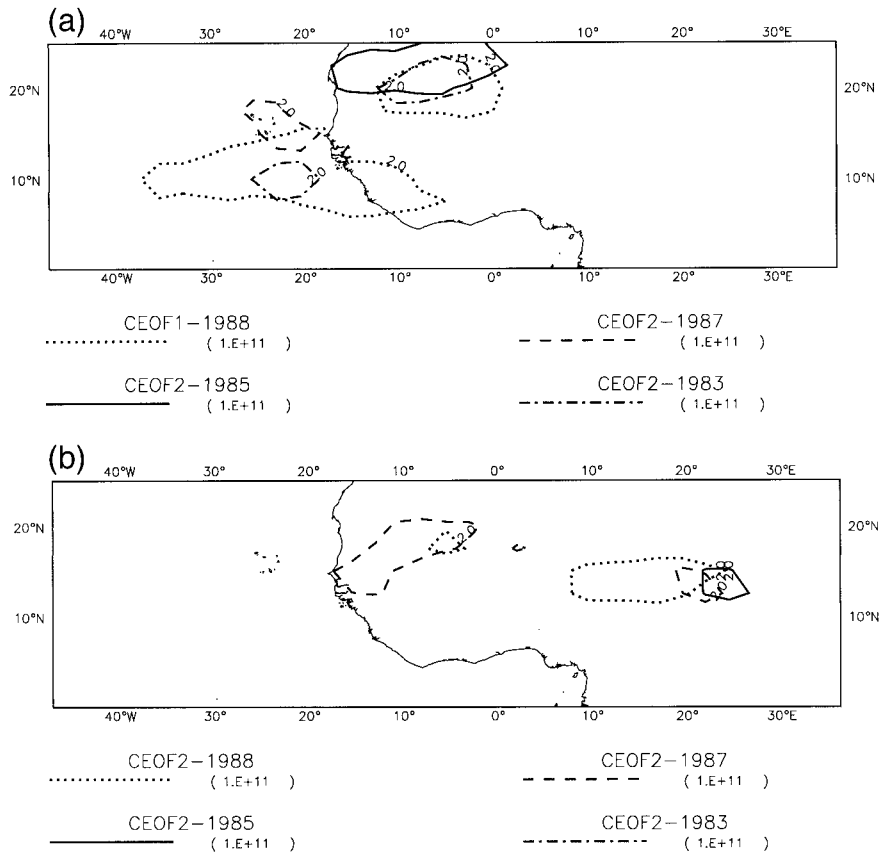

FIG. 15. Schematic space representation of the time variance for the years 1983, 1985, 1987, and 1988 for the mode 2 of filtered vorticity at 850 hPa; (a) ECMWF, (b) CNRM GCM. Contour interval is 2×10^{-11} s^{-2}.

data (see Figs. 16a,b) exhibits clearly some deficiencies of the model. On the PC1 time series of the analyses, one can see the low-frequency modulation previously shown on CPC1. The GCM time series indicates that, in 1985, the model started later in comparison with the analyses. Except for this discrepancy, the amplitudes of the GCM time series are comparable to those of the analysis time series. This kind of problem is not constant and depends on the year. For example, in 1988 the model started at the right time, but the synoptic scale activity (i.e., AEWs) was slightly less. However, the phase of the low-frequency modulation was quite well reproduced in comparison with 1985.

As stated in the introduction, there is probably an interesting development for the future. It concerns the understanding of the physical or dynamical processes

TABLE 4. Latitudes and longitudes of the maxima of variance for ECMWF modes and GCM modes for the different years.

Year	1982	1983	1984	1985	1986	1987	1988
ECMWF	17.5°N	18°N	17°5′N	19°N	17°N	12°N	19°N
Mode 1	5°W	7°W	4°W	11°W	15°W	8°W	3°W
AMIP	10.5°N	12°5N	15°N	13°N	17°N	16°N	15°N
Mode 1	12°W	13°W	9°W	9°W	13°W	1°E	13°W
ECMWF	17°N	20°N	21°N	22°N	22°N	16°N	20°N
Mode 2 (2 cells)	5°E	6°W	6°W	5°W	5°W	22°W	6°W
	12°N	10°N	10°N	10°N	11°N	13°N	12°N
	23°W	21°W	16°W	29°W	34°W	6°E	20°W
AMIP	24°N	18°N	17°N	17.5°N	15°N	13°N	15°N
Mode 2 (2 cells)	15°E	3°E	21°E	2°E	7°E	21°E	18°E
	14°N	13°N	17°N	12°N	17.5°N	17°5′N	18°N
	9°W	21°E	4°E	24°W	15°E	10°W	5°W

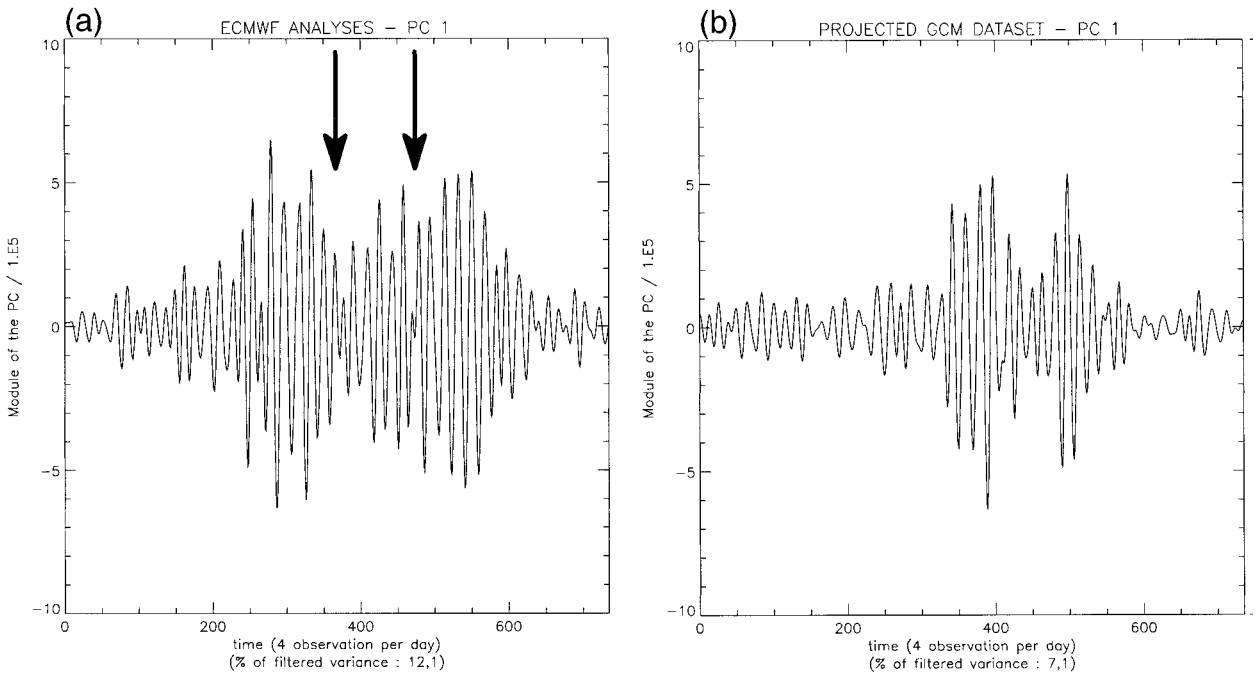

FIG. 16. Time series of the first PC of filtered vorticity at 850 hPa (s^{-2}) for the year 1985; (a) ECMWF, (b) projected CNRM GCM data. Arrows indicate the low-activity phase.

involved in this low-frequency modulation and consequently the needed GCM improvements to duplicate the right phase of this modulation in the frame of a dynamical extended-range forecast. This modulation could probably be in close relationship with an expected intraseasonal modulation of rainfall over West Africa, as mentioned earlier.

Finally, the maps in Figs. 17a and 17b highlight the influence of the quality of the time representation of phenomena in the GCM. One has to remember here that the patterns are the same in analyses and in GCM because we use the projected GCM dataset. The differences in CEOFs and consequently in patterns of time variance are partly due to the differences in the temporal representation between the two datasets. The two maps shown in Fig. 17 correspond to CPC1 and CPC2 of the projected GCM dataset. One can see that the discrepancy in space representation of AEW tracks is quite similar to the one previously shown (see section 4a). So it seems that the quality of the time representation of phenomena in the model is able to influence the kind of space representation problems seen in the GCM. More precisely, we could propose that the time representation failure of the GCM leads to main variability modes in the GCM that probably exist in the analyses but with no great significance compared to their main variability modes.

5. Summary and conclusions

The aim of this study has been to investigate the ability of the CNRM GCM (Emeraude) to reproduce the AEW space–time variability with the help of two complementary objective methods: a space–time spectral analysis and a complex empirical orthogonal function analysis. These two methods are complementary in the sense that while the former makes use of Fourier's functions, the latter uses an empirical approach to calculate the space–time variance. Further, the latter method can be advantageously applied to space–time filtered data, in a spectral window determined by the former method. The CEOF analysis goes deeply into the space–time variability aspects, giving several modes of variability sorted according to a criterion of variance maximum. These methods have been particularly relevant to reaching the goal of this study in the sense that they have provided a synthetic and quantitative view of the variability of both analyses and simulated data. Particularly looking at the low-frequency modulation revealed in this paper, this result would have been more difficult to achieve with more simple methods.

Relative vorticity at 850 hPa has been used in this study. Specifically, 6-hourly data have been extracted during the six months of the African summer monsoon (May–October) for the years 1982–88, over a limited area enclosing Africa and the eastern Atlantic Ocean, north of 10°S. Simulated data were produced by a 10-yr run (1979–88) of the CNRM GCM Emeraude, part of the AMIP experiment. Analyzed data have been obtained from the ECMWF.

As a first step, we have studied more deeply the year 1985 in order to calibrate the use of the methods and to validate the results and attempt possible interpreta-

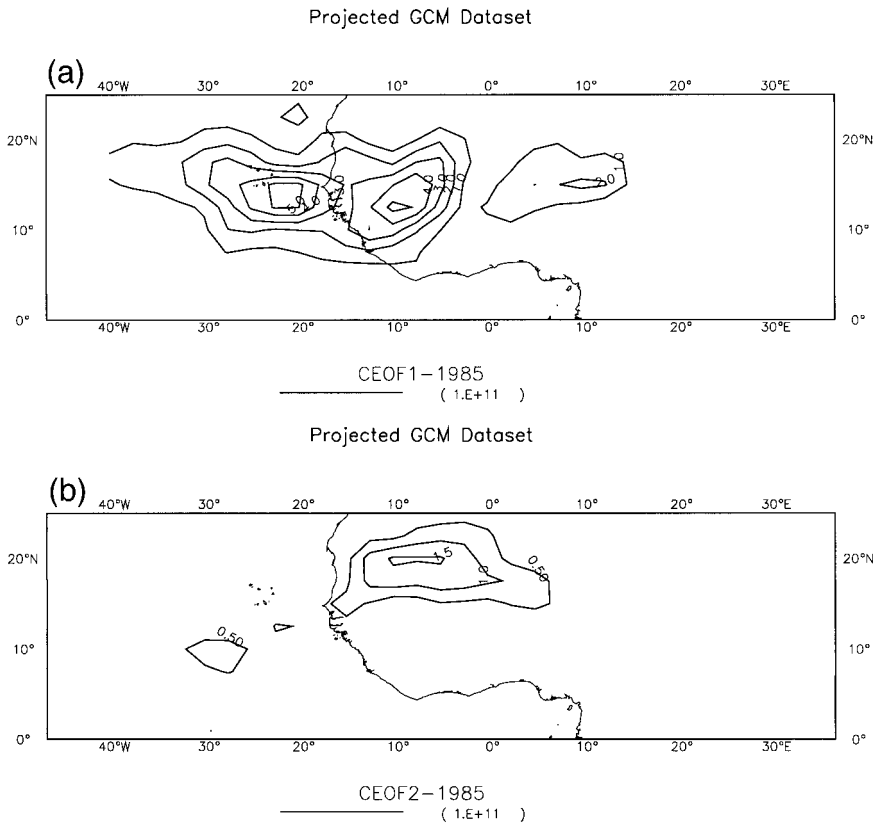

FIG. 17. Space representation of the time variance of CPCs (s^{-2}) for the year 1985 from the projected CNRM GCM data; (a) first CPC. Contour interval is 10^{-11} s^{-2}, (b) second CPC. Contour interval is 0.5×10^{-11} s^{-2}.

tion. Then we have processed the other years in order to address the interannual variability and verify the stability of the results and interpretations.

The STSA has shown that the model exhibits the same kind of power density pattern as the one given by the analysis in the AEW space–time spectral window (i.e., 3–5 days and 2200–4400 km) for westward propagating phenomena. Both in the model and in the analysis, more than 70% of the cumulated variance in this spectral window is due to traveling wave variance. However, the variance maximum of the model tends to be located toward lower frequencies, compared to the variance maximum of the analysis. This means that the simulated AEWs have a weaker phase speed than the analyzed AEWs, as already noted by other authors (Reed et al. 1988b; Druyan and Hall 1994). This discrepancy might be due to the weak shear of the simulated AEJ, because of the rather low resolution of the model.

With the help of the STSA, it has been possible to calculate, at each grid point and for each month, the time variance for westward traveling oscillations in the AEW space–time spectral window. The spatial patterns of these variance fields enabled us to discuss the AEW tracks given by the location of the variance maxima as well as their intraseasonal variability. There is a qualitative agreement between the simulation and the analysis in terms of the seasonal evolution of the location and intensity of the variance maximum. The largest variance occurs most of the time in August, with an essentially latitudinal displacement of the tracks toward the north from June to July and toward the southwest from August to September; the variance maximum is located most of the time over the western edge of the African continent, except for September where the maximum tends to be over the Atlantic Ocean. However, there is more variance east of 10°E in the model. On the other hand, the most important failure of the model is the fact that it produces one main AEW track that is located between the two tracks revealed by the analysis. This failure has been partly corrected in the following release of the CNRM GCM through the introduction of a new surface processes parameterization scheme and by an increase of the albedo values over the Sahel. These model modifications resulted in a southward shift of precipitation–AEJ–AEW tracks.

Finally, space–time cross-spectrum analysis of the couples (u, v) and (v, T) in the AEW spectral window has shown a rather good resemblance between the analyzed and simulated patterns. Indeed, the barotropic conversion of kinetic energy from the AEJ to the waves

seems to be larger off the coast of West Africa, while the baroclinic conversion of the potential energy from the AEJ to the waves seems to be larger over land, as already indicated by Norquist et al. (1977).

The CEOF analysis has exhibited two main modes of variability, a northern single-track mode (mode 1) and a dual-track mode (mode 2), which seem to compose notably AEWs characterized, respectively, by dynamical effects and by diabatic effects. This distinction between the two modes is consistent with previous studies and known properties of AEWs, particularly those moving in the southern part of West Africa. But it is only speculative and should be investigated further. Notably, this interpretation could be more precisely validated using local methods instead of global methods. Of course, rotation methods could be useful for the years (such as 1987) where the patterns are mixed too much. The modes produced by the model are closer in space to each other than the modes produced by the analysis (this is coherent with the two preferred tracks in the analysis, mentioned previously). The period of the dual-track mode (period around or less than 4 days) seems to be less than that of the northern single-track mode, and the simulated AEW periods are larger than those of the analyzed AEWs. The time series of the complex principal components present a seasonal modulation and, interestingly, an intraseasonal modulation. The latter modulation, which is statistically significant (by comparison with a red-noise spectrum) has a period of about 40–50 days for the first CPC and 20–40 days for the second CPC. This intraseasonal modulation is qualitatively well described by the model. However, an understanding of this phenomenon needs further studies.

The interannual variability of the two modes is not too badly reproduced by the model in terms of the cumulated variance of these modes. This conclusion has also been obtained with the help of the STSA. The space patterns of the two modes of ECMWF show a good stability of the latitudinal location of the maxima of variance (except 1987). The particular behavior for this year is not reproduced by the model. Interestingly, for the year 1988, which was the wettest of the period, mode 2 (composing notably AEWs characterized by diabatic effects and a significant southerly component) presents more variance than mode 1, both in the model and the analysis. This might be linked to the fact that the large-variance AEWs tend to be correlated with large cloud clusters (e.g., Toledo Machado at al. 1993). However, unfortunately for this version of the CNRM GCM, the reproduction of mode 2 is worse than that of mode 1 in terms of variance patterns and periods.

The projection of the simulated data on the analyzed eigenvectors has allowed a rigorous comparison of the time series of the principal components in the sense that the data are decomposed on the same space vectors. Thus, in 1985, the model has started the activity of the AEWs later than the analysis, while in 1988 the activity phasing was good but the amplitude of the simulated AEWs was too weak. By carrying out a CEOF analysis of the model-projected data, it has been shown that the time misrepresentation of the GCM could partly be quoted as an explanation of its space representation failure.

As we have shown in this paper that the CNRM GCM was able to reproduce some characteristics of the AEW space–time variability, despite several discrepancies among which the track location failure has already been partly corrected, the next step would be to study the ability of the model to forecast the phase of the AEW low-frequency modulation. At the same time, the ongoing impovements of the physical parameterizations will undoubtly help to overcome some of the GCM errors discussed in this paper. It would also be interesting to understand the causes of this low-frequency modulation and, on the other hand, to determine the possible quality of statistical relationships between the amplitude of different meteorological fields modulated by the AEWs, and the precipitation field.

Acknowledgments. This research has been accomplished at the Ecole Nationale de la Météorologie, Toulouse, France. We gratefully acknowledge helpful suggestions offered by anonymous reviewers. Dr. R. K. Kolli provided very able assistance in the improvement of the English in the manuscript.

REFERENCES

Albignat, J. P., and R. J. Reed, 1980: The origin of African wave disturbances during phase III of GATE. *Mon. Wea. Rev.,* **108,** 1827–1839.

Barnett, T. P., 1983: Interaction of the monsoon and Pacific trade wind system at interannual time scales. Part I: The equatorial zone. *Mon. Wea. Rev.,* **111,** 756–773.

Bloomfield, P., and J. M. Davis, 1994: Orthogonal rotation of complex principal components. *Int. J. Climatol.,* **14,** 759–775.

Burpee, R. W., 1972: The origin and structure of easterly waves in the lower troposphere of North Africa. *J. Atmos. Sci.,* **29,** 77–90.

——, 1974: Characteristics of North African easterly waves during the summers of 1968 and 1969. *J. Atmos. Sci.,* **31,** 1556–1570.

——, and R. J. Reed, 1982: Synoptic scale motions. *The GATE Monograph,* Garp Publ., No. 25, WMO/ICSU, 61–120.

Carlson, T. N., 1969a: Synoptic histories of three African disturbances that developed into Atlantic hurricanes. *Mon. Wea. Rev.,* **97,** 256–276.

——, 1969b: Some remarks on African disturbances and their progress over the tropical Atlantic. *Mon. Wea. Rev.,* **97,** 716–726.

Céron, J. P., and J. F. Guérémy, 1994: Numerical sensitivity studies on the West African monsoon: Initial conditions and land processes. *Proc. Int. Conf. on Monsoon Variability and Prediction,* Vol. 2, WCRP-84, WMO-TD 619, Trieste, Italy, WMO, 47–479.

Déqué, M., 1986: Analyse en composantes principales complexes. Note de travail de l'Etablissement d'Etudes et de Recherches Météorologiques, 152, 59 pp. [Available from Météo-France—CNRM/GMGEC, F31057 Toulouse, France.]

Desbois, M., T. Kayiranga, B. Gnamien, S. Guessous, and L. Picon, 1988: Characterization of some elements of the Sahelian climate and their interannual variations for July 1983, 1984 and 1985 from the analysis of METEOSAT ISCCP data. *J. Climate,* **1,** 867–904.

Druyan, L. M., and T. M. Hall, 1994: Studies of African wave disturbances with the GISS GCM. *J. Climate,* **7,** 261–276.

Duvel, J. P., 1990: Convection over tropical Africa and Atlantic Ocean during northern summer. Part II: Modulation by easterly waves. *Mon. Wea. Rev.,* **118,** 1855–1868.

ECMWF, 1988: Data assimilation and the use of satellite data. *ECMWF Seminar Proceedings*, Vol. 1, Reading, United Kingdom, ECMWF, 314 pp.

Estoque, M. A., J. Shukla, and J. G. Jiing, 1983: African wave disturbances in a general circulation model. *Tellus,* **35A,** 287–295.

Gates, W. L., 1992: AMIP: The Atmospheric Model Intercomparison Project. *Bull. Amer. Meteor. Soc.,* **73,** 1962–1970.

Hastenrath, S., 1991: *Climate Dynamics of the Tropics.* Kluwer Academic, 488 pp.

Hayashi, Y., 1977: On the coherence between progressive and retroprogressive waves and a partition of space time power spectra into standing and traveling parts. *J. Appl. Meteor.,* **16,** 368–373.

——, 1979: A generalized method of resolving transient disturbances into standing and traveling waves by space-time spectral analysis. *J. Atmos. Sci.,* **36,** 1017–1029.

——, 1982: Space time spectral analysis and its applications to atmospheric waves. *J. Meteor. Soc. Japan,* **60,** 156–171.

Horel, J. D., 1984: Complex principal component analysis: Theory and examples. *J. Climate Appl. Meteor.,* **23,** 1660–1673.

Jenkins, G. M., and D.G. Watts, 1968: *Spectral Analysis and Its Applications.* Holden-Day Series, 517 pp.

Lare, A. R., and S. E. Nicholson, 1994: Contrasting conditions of surface water balance in wet years and dry years as a possible land surface–atmosphere feedback mechanism in the West African Sahel. *J. Climate,* **7,** 653–668.

Mahfouf, J. F., 1993: L'expérience d'intercomparaison AMIP: Simulation du climat 1979 1988 avec le modèle Emeraude. Note de travail du groupe de météorologie de grande échelle et climat 18, 32 pp. [Available from Météo-France—CNRM/GMGEC, F31057 Toulouse, France.]

Mass, C., 1979: A linear primitive equation model of African wave disturbances. *J. Atmos. Sci.,* **36,** 2075–2092.

Murakami, M., 1979: Large-scale aspects of deep convective activity over the GATE area. *Mon. Wea. Rev.,* **107,** 994–1013.

Nitta, T., and Y. Takayabu, 1985: Global analysis of the lower tropospheric disturbances in the tropics during the northern summer of the FGGE year. Part II: Regional characteristics of the disturbances. *Pure Appl. Geophys.,* **123,** 272–292.

Norquist, D. C., E. E. Recker, and R. J. Reed, 1977: The energetics of African wave disturbances as observed during the phase III of GATE. *Mon. Wea. Rev.,* **105,** 334–342.

Paradis, D., J.-P. Lafore, J.-L. Redelsperger, and V. Balaji, 1995: African easterly-waves and convection. Part I: Linear simulations. *J. Atmos. Sci.,* **52,** 1657–1679.

Payne, S. W., and M. M. McGarry, 1977: The relationship of satellite convective activity to easterly waves over West Africa and the adjacent ocean during phase III of GATE. *Mon. Wea. Rev.,* **105,** 413–420.

Reed, R. J., D. C. Norquist, and E. E. Recker, 1977: The structure of African wave disturbances as observed during phase III of GATE. *Mon. Wea. Rev.,* **105,** 317–333.

——, A. Hollingsworth, W. A. Heckley, and F. Delsol, 1988a: An evaluation of the performance of the ECMWF operational system in analyzing and forecasting easterly wave disturbances over Africa and the tropical Atlantic. *Mon. Wea. Rev.,* **116,** 824–865.

——, E. Klinker, and A. Hollingsworth, 1988b: The structure and characteristics of African easterly wave disturbances as determined from the ECMWF operational analysis/forecast system. *Meteor. Atmos. Phys.,* **38,** 22–33.

Rennick, M. A., 1976: The generation of African waves. *J. Atmos. Sci.,* **33,** 1955–1969.

Saloum, M., 1993: Analysis of rain producing systems over Sahel region during the wet and dry period. *Proc. First Int. Conf. of African Meteorological Society,* Nairobi, Kenya, African Meteorological Society, 122–138.

Shaw, D. B., P. Lönnberg, A. Hollingsworth, and P. Undén, 1987: Data assimilation: The 1984/85 revisions of the ECMWF mass and wind analysis. *Quart. J. Roy. Meteor. Soc.,* **113,** 533–566.

Shove, D. J., 1946: A further, contribution to the meteorology of Nigeria. *Quart. J. Roy. Meteor. Soc.,* **72,** 105–110.

Thorncroft, C. D., and B. J. Hoskins, 1994a: An idealized study of African easterly waves. I: A linear view. *Quart. J. Roy. Meteor. Soc.,* **120,** 953–982.

——, and ——, 1994b: An idealized study of African easterly waves. II: A nonlinear view. *Quart. J. Roy. Meteor. Soc.,* **120,** 983–1015.

Tiedke, M., W. A. Heckley, and J. Slingo, 1988: Tropical forecasting at ECMWF: The influence of physical parameterization on the mean structure of forecasts and analyses. *Quart. J. Roy. Meteor. Soc.,* **114,** 639–664.

Toledo Machado, L. A., J. P. Duvel, and M. Desbois, 1993: Diurnal variations and modulation by easterly waves of the size distribution of convective cloud clusters over West Africa and the Atlantic Ocean. *Mon. Wea. Rev.,* **121,** 37–49.

Unden, P., 1989: Tropical data assimilation and analysis of divergence. *Mon. Wea. Rev.,* **117,** 2495–2517.

Walker, J., and P. R. Rowntree, 1977: The effect of soil moisture on circulation and rainfall in a tropical model. *Quart. J. Roy. Meteor. Soc.,* **103,** 29–46.

Wallace, J. M., and R. E. Dickinson, 1972: Empirical orthogonal representation of time series in the frequency domain. Part I: Theoretical considerations. *J. Appl. Meteor.,* **11,** 887–892.